Cold Surges in Tropical and Extratropical South America: The Strong Event in June 1994

JOSE MARENGO, ANGEL CORNEJO, PRAKKY SATYAMURTY, AND CARLOS NOBRE

Centro de Previsão de Tempo e Estudos Climáticos, CPTEC/INPE, Sao Paulo, Brazil

WILLIAM SEA

Department of Soil, Water and Climate, University of Minnesota, St. Paul, Minnesota

(Manuscript received 5 March 1996, in final form 1 February 1997)

ABSTRACT

The authors investigate one case of surges of polar air that occasionally propagate into southeastern Brazil during wintertime and are harmful to coffee production because of the freezing conditions associated with them. The cooling is also observed in southern and, with less intensity, in western Amazonia. The event of 26 June 1994 is studied. The frost event caused a sharp drop in coffee production and similarly dramatic increases in coffee prices.

The event was characterized by the presence of an anticyclonic perturbation off the coast of Chile that enters South America and crosses the Andes Mountains south of 45°S hours later. The anticyclone center tracks equatorward until it reaches 20°–30°S and then shifts eastward toward the Atlantic.

Based on a diagnostic analysis using the National Centers for Environmental Prediction–National Center for Atmospheric Research (NCEP–NCAR) reanalysis, a two-stage process can be distinguished. In the starting period, midtropospheric troughing is established east of the Andes, over central Argentina, due to stretching and/or vorticity advection. This troughing is responsible for cold advection along the eastern flank of the Andes, which produces substantial temperature drops and deepens the upper trough locally. The increase in the magnitude of the zonal temperature gradients east of the cold advection zone at levels near 700 hPa is another result of the cooling process. This feature would ensure that the cold advection be extended eastward, producing an upper-level trough local deepening there. This intensification would produce an increase in the cyclonic vorticity advection, which would tend to produce sea level pressure drops underneath. This near-surface low pressure area would eventually contribute to the southeastern Brazil (SB) cooling due to the associated southerly winds.

Another feature is the near-surface local anticyclonic generation due to midtropospheric cold advection associated with descending motions, low-level divergence, and anticyclonic growth. Eventually this high pressure would also contribute to produce southwesterlies to transport cold air to SB.

The paper is divided in two sections. The first part is a study of synoptic and climatic aspects of the cold surge episodes by using daily surface climatic observations. The purpose of the second part is to analyze the dynamic aspects of this cold episode and to study the cooling mechanisms by using the four-times-daily surface and upper-air NCEP–NCAR reanalysis, as well as to look for possible predictors.

1. Introduction

Freezing weather in southern Brazil is caused by outbreaks of polar air during wintertime (May–August). These cold surges occur several times a year (from zero to eight), producing low temperatures in midlatitudes, and are sometimes so strong that extensive freezes affect southern Brazil with considerable cooling in central and northern Amazonia (Serra and Ratisbona, 1942; Parmenter 1976; Satyamurty et al. 1990; Seluchi and Nery 1992; Marengo et al. 1997). The freezing temperatures and frost affect a large part of the harvests of wheat, coffee, soybeans, and oranges in the agricultural lands of southeastern Brazil (SB).

a. Cold surges in South America and their impacts on coffee production

The current available literature about South American cold surges documents the weather evolution during particular events that affected Amazonia and the coffee-growing areas of southeastern Brazil. The following are some episodes of cold surges that affected southeastern Brazil and in some cases produced cooling in Amazonia. Listed also are some references of studies of these cold events:

1928 and 1957 (Myers 1964); 1963 (Brinkmann et al. 1971; Brinkmann and Goes-Ribeiro 1971, 1972); 1975

Corresponding author address: Dr. José Marengo, CPTEC/INPE, Rodovia Presidente Dutra Km. 40, 12630-000 Cashoeira Paulista, Sao Paulo, Brazil.

(Parmenter 1976; Tarifa et al. 1977; Girardi 1983; Marengo 1984); 1972 (Hamilton and Tarifa 1978); 1979 and 1981 (Haddock et al. 1981; Fortune and Kousky 1983); 1988 (Dapozzo and Silva Dias 1994); 1989 (Seluchi and Nery 1992); and 1990 (Satyamurty et al. 1990).

Seluchi and Nery (1992) and Algarbe and Cavalcanti (1994) have described a climatology of events during several years and characterized the cold events according to different methodologies. Several of these articles have dealt with descriptive aspects of cold surges, while a few of them have analyzed events from a dynamic point of view, looking for the physical mechanisms responsible for their evolution, with the final goal of better monitoring and prediction. A typical weather evolution during a cold surge, or friagem, as they are referred to in Brazil,[1] is as follows. A transient cold core high pressure center moves onto the southern tip of South America from the Pacific Ocean, then intensifies while crossing Argentina 2–3 days later, becoming quasi-stationary over the large Brazilian coffee region in the southeastern part of the country. These processes occur 3–4 days after the front has passed the southern tip of South America. Cooling is usually preceded by an increase in surface pressure and a reduction in atmospheric humidity. In Amazonia, the air temperature is markedly high during the day with clear skies. The temperature begins to drop at night while the pressure increases; sometimes the changes amount to 15°C and 18 hPa in 24 h. In some locations, the wind becomes strong from the south. The average duration of a cold surge is 5–6 days.

South and Central America produce the majority of coffee traded in world commerce. Brazil and Colombia, the largest growers of arabica coffee, accounted for about 43% of the world's green coffee production for the 1993–94 crop year, as indicated by the New York Coffee, Sugar, and Cocoa Exchange, Inc. (CSCE). Historically, weather has played a major role in determining the world supply. Large production increases after recovery from the 1953 Brazilian frost created large price declines. Likewise, the Brazilian frosts in June and July 1994 caused a sharp drop in coffee production and dramatic increases in coffee prices (according to CSCE). Reports issued by the U.S. Department of Agriculture (USDA) indicated that the freeze of July 1975 (perhaps the most intense in this century) reduced the 1976–77 harvest to 9.3 million bags (60 kg per bag), compared to the 1961–80 average of 19 million bags. Estimates of losses in 1995 due to the frosts of June and July 1994 are shown in Table 1. Marshall (1983) listed the following as cold events that produced intense damage in the coffee growing areas of southern and southeastern Brazil:

14 July 1882, 16 July 1894, 25 July 1895, 5 July 1898, 18 June 1899, 19 August 1902, 12 August 1904, 18 July 1910, 23 June 1911, 3 September 1912, 25 June 1918, 25 June 1928, 29 June 1931, 14 July 1933, 12 June 1942, 15 September 1943, 5 July 1953, 2 August 1955, 21 July 1957, 7 July 1962, 22 June 1963, 28 June 1964, 21 August 1965, 6 August 1966, 11 July 1969, 9 July 1972, 18 July 1975, 15 August 1978, 31 May 1979, and 18 July 1981.

From our own compilations, we have updated this list to 1996:

28 July 1982, 15 June 1983, 3 August 1983, 24 August 1984, 8 June 1985, 2 June 1986, 26 July 1986, 26 July 1988, 7 July 1989, 22 July 1990, 24 July 1992, 15 July 1993, 1 August 1993, 26 June 1994, 9 July 1994, and 10 August 1994.

No events damaging the coffee agriculture in the region were detected in 1995 and 1996.

The strong cold event of 26 June 1994 was very interesting from an operational point of view. Since there was a significant delay in the forecasts from the meteorological agencies in Brazil, the New York and London Stock Exchanges reacted quicker than the Brazilian one. Heavy speculation resulted in coffee prices increasing almost 70% in a few days in the CSCE (Table 2). Given the intensity of this particular event, we wish to understand why this phenomenon evolved into an intense event that was ruinous to coffee production and why it featured a greater equatorward penetration of cold air than other events.

Descriptions of cold air outbreaks in South America, particularly with attention to contributing physical mechanisms, are lacking in the literature. Our work attempts to fill this gap. Fortune and Kousky (1983) found some important features preceding freezing tempera-

TABLE 1. Coffee production (in millions of bags) in the southern states of Brazil from 1990 to 1996 (estimates for 1995 and 1996). Each bag contains 60 kg of the product. Source: Foreign Agriculture Service, Tropical Agricultural Circular, U.S. Department of Agriculture.

	Year						
State	1990–91	1991–92	1992–93	1993–94	1994–95	1995–96[a]	1995–96[b]
Minas Gerais	9.1	13.5	9.5	13.0	13.0	15.5	8.0–9.0
São Paulo	9.5	4.0	5.2	5.5	4.0	5.0	2.0–2.5
Esprito Santo[c]	5.2	5.5	5.0	4.5	4.0	5.0	3.0–3.5
Paraná	4.0	2.5	1.8	3.0	2.0	2.0	0.2
Others	3.2	3.0	2.5	2.5	3.0	2.5	2.5
Total Brazil	31.0	28.5	24.0	28.5	26.0	30.0	15.7–17.7

[a] Prefrost estimate.
[b] Postfrost estimates as speculated during December 1994.
[c] Most of the reduction in Espirito Santo was caused by drought conditions rather than frost.

[1] These cold events, like the friagem in Amazonia, have several regional names, such as norte, chocolatero, and tehuano in Mexico; papagayo in Nicaragua and Guatemala; atemporalado in Honduras; and invierno de las Chicharras in Venezuela.

TABLE 2. Prices of coffee traded at the Coffee, Sugar, and Cocoa Exchange, Inc., of New York for the period 20 June–7 July. Numbers represent opening price for the market on business days. The prices are in U.S. dollars per pound of coffee. The day in which the freeze struck is indicated with an asterisk.

Day	Price
20 June	1.327
21 June	1.295
22 June	1.313
23 June	1.264
24 June	1.300
25 June	Saturday
26 June*	Sunday
27 June	1.750
28 June	1.680
29 June	1.705
30 June	1.890
1 July	1.973
2 July	Saturday
3 July	Sunday
4 July	Holiday
5 July	1.873
6 July	1.885
7 July	1.948

tures in Brazil, such as a slowly moving long-wave pattern in the central South Pacific Ocean that amplified before the cold event. They also pointed out the presence of an intense upper-level ridge and trough in southern Chile and eastern Brazil, respectively, which favored the equatorward channeling of cold air. However, they did not address the physical cause for such intensification. The same is true for Hamilton and Tarifa (1978), who described a cold event in 1972. They also found several features, similar to the ones presented in this report, that preceded the cold episode, such as an equatorward air current channeled between the Brazilian plateau and the Andes, a midtropospheric trough east of the mountains, and a cold-core low-level anticyclone near the cold region.

Thus, the current study analyzes the surface and upper-air weather conditions for the cold surge event of 26 June 1994 to characterize and quantify this phenomenon. Our specific goals are to (a) describe this episode with emphasis on the impacts of weather conditions from the Amazon Basin to southern Brazil during and prior to the coldest days, (b) assess the spatial extension of the cooling over those regions, and (c) identify the physical mechanisms responsible for its evolution as well as possible predictors of this phenomenon.

b. Cold surges in other regions of the Americas

In North America, similar events have been reported, and even though the changes in the pressure, temperature, and intensity of the cold anticyclone may be much higher than in South America, the physical mechanisms are similar, especially regarding the effect of a mountain barrier in the initiation and evolution of the phenomena. Severe Florida citrus freezes since 1880 have been studied by Rogers and Rohli (1991) and have been associated with polar anticyclone outbreaks in the plains of southern Canada and the United States. An outbreak of bitterly cold polar air, moving equatorward across the plains of North America, precedes each Florida citrus freeze. Colle and Mass (1995) have documented northerly surges of cold air that often move equatorward along the eastern side of the Rockies from southern Canada into Mexico and have described the strongest surges that developed in the midwinter of 1994 with temperature decreases of 20°–30°C and pressure rises of 15–30 hPa in 24 h. These cold events are usually accompanied by a meridionally elongated pressure ridge and a strong low-level ageostrophic wind that parallels the mountain, similar to cold waves in South America.

Recently, Schultz et al. (1997) studied a cold surge that originated in the wake of the U.S. superstorm of 12–14 March 1993. The cold surge, which originated over Alaska and western Canada, brought northerlies exceeding 20 m s^{-1} and temperature decreases up to 15°C over 24 h into Mexico and Central America. The event initiated as a developing cyclone in the south-central United States, causing an along-barrier pressure gradient to form northerlies, forcing topographically channeled northerlies along the Rocky Mountains and the Sierra Madre to transport cold air equatorward. The nature of topographically trapped cold surges in North America has been documented elsewhere [see reviews in Colle and Mass (1995)]. At the synoptic scale, this cold surge was forced equatorward mainly by an upper-tropospheric trough and by topographic channeling similar to cold-air damming.

As will be indicated in later sections, the Andes may play an important role in the initial stages by helping the equatorward advance of the surface high pressure system, due to the effect of the elevated terrain of the mountains on the circulation of the anticyclone.

Many studies have also examined features associated with cold outbreaks, especially the development of a surface anticyclone upstream of the cold region. Colucci and Davenport (1987) found that cold anticyclones were present downstream of amplifying 500-hPa ridges and most were followed by a 500-hPa trough amplification and a cold outbreak episode. Although they used the quasigeostrophic height tendency equation for the diagnosis of the events, the physical mechanisms for the evolution were not completely identified.

Konrad and Colucci (1989) described the thermodynamic aspects of two strong episodes in North America. An intense cold air advection between a cyclone–anticyclone pair in eastern North America was found during the events, although they indicated that the cyclone does not seem to be crucial for the cooling.

2. Data and analysis

In this study, for the 23–28 June 1994 period, we used the global reanalysis produced by the National

Centers for Environmental Prediction (NCEP) and the National Center for Atmospheric Research (NCAR), known as the NCEP–NCAR reanalysis (Kalnay et al. 1996). Six-hourly surface and upper-air (1000, 925, 850, 700, 600, 500, and 300 hPa) information were used with a 2.5° × 2.5° latitude–longitude physical grid spacing. This dataset has been provided by the National Oceanic and Atmospheric Administration (NOAA) Climate Diagnostics Center, Boulder, Colorado. The extent of cloudiness associated with the cold surges studied here was determined from specially enhanced infrared (IR) images from the Geostationary Observational Environmental Satellite (GOES), provided by the Instituto Nacional de Pesquisas Espaciais (INPE), São Paulo, Brazil. The images were taken at 1200 UTC and were available for the period between 24 and 28 June 1994.

Cold outbreaks during the period 1985–93 were analyzed by accessing the gridded (2.5° × 2.0°) National Aeronautics and Space Administration (NASA)–GEOS 6-h reanalysis in a South American domain. The NASA–GEOS is a multiyear global assimilated dataset with version 1 of the Goddard Earth Observing System (GEOS-1 Data Acquisition System), produced by the Data Assimilation Office at Goddard Space Flight Center, and is described in Schubert et al. (1993).

Additional information included surface weather charts during 26 June 1994, the coldest day, produced by CPTEC and INMET (National Institute of Meteorology from Brazil). This information, together with the NCEP–NCAR reanalyses, was used to map trajectories of the cold-core anticyclone as well as the advance of the cold front from formation to dissipation. Daily information of sea level pressure, winds, dewpoint temperature, station pressure, and minimum temperatures for Brazilian and Peruvian stations before and during the days with cold surges was provided by the National Climatic Data Center, Asheville, North Carolina, and the Meteorological System of Paraná (SIMEPAR) in Paraná, Brazil. SIMEPAR had observations at 0900, 1500, and 2100 LT, as well as extreme air temperatures. In addition, we used hourly and daily observations of air temperature, dewpoint, total incoming solar radiation, and wind speed and direction from the archives of the Anglo–Brazilian Amazon Climate Observation study (ABRACOS; Gash et al. 1996) for the sites shown in Fig. 1: Fazenda Dimona (nearby Manaus, central Amazonia), Fazenda Nossa Senhora da Aparecida (nearby Ji-Paraná, southwestern Amazonia), and Fazenda Boa Sorte (nearby Marabá, eastern Amazonia).

The NCEP–NCAR reanalyses at the surface and upper air are interpreted using quasigeostrophic theory. The vorticity and thermodynamic equations are used in several steps of the analysis to identify mechanisms for the observed changes. Ignoring diabatic effects, the thermodynamic energy equation in isobaric vertical coordinates can be written as

$$\frac{\partial T}{\partial t} = -u\frac{\partial T}{\partial x} - v\frac{\partial T}{\partial y} + w\left(\frac{\alpha}{C_P} - \frac{\partial T}{\partial p}\right) = \text{HTADV} + (\text{ADIAB} + \text{WADV}), \quad (1)$$

where u and v are the horizontal wind components in the zonal and meridional directions, w is the wind component in the vertical direction, T is temperature, p is pressure, C_p is the isobaric specific heat, and a is the specific volume. The local change is an approximation by forward time differencing ($\Delta t = 6$ h). The horizontal advection term (HTADV) is calculated using centered differencing on pressure surfaces. The first and second terms on the right-hand side conform to the HTADV, while the third and fourth are the adiabatic heating (ADIAB) and vertical temperature advection (WADV) terms, respectively. The following approximate vorticity equation was used:

$$\frac{\partial \zeta}{\partial t} = -\mathbf{V}_h\cdot\boldsymbol{\nabla}(\zeta + f) + (\zeta + f)\frac{\partial w}{\partial p}, \quad (2)$$

where the first term on the right-hand side is the advection of absolute vorticity (HVOAD) and the second is the generation of vorticity caused by horizontal divergence (DIVTERM).

To diagnose the geopotential height field we used the geopotential tendency equation (Holton 1992), which for future reference will be written as

$$\left(\nabla^2 + \frac{f_o^2}{\sigma}\frac{\partial^2}{\partial p^2}\right)\chi = -f_o\mathbf{V}_g\cdot\boldsymbol{\nabla}\left(\frac{1}{f}\nabla^2\Phi + f\right) + \frac{f_o^2}{\sigma}\frac{\partial}{\partial p}\left(-\mathbf{V}_g\cdot\boldsymbol{\nabla}\frac{\partial\Phi}{\partial p}\right); \quad \text{A} = \text{B} + \text{C}. \quad (3)$$

The quasigeostrophic (QG) omega equation (Holton 1992) will also be used for diagnosing the vertical velocity field. For future reference it will be written as

$$\left(\nabla^2 + \frac{f_o^2}{\sigma}\frac{\partial^2}{\partial p^2}\right)\omega = \frac{f_o^2}{\sigma}\frac{\partial}{\partial p}\left[\mathbf{V}_g\cdot\boldsymbol{\nabla}\left(\frac{1}{f_o}\nabla^2\Phi + f\right)\right] + \frac{1}{\sigma}\nabla^2\left[\mathbf{V}_g\cdot\boldsymbol{\nabla}\left(-\frac{\partial\Phi}{\partial p}\right)\right], \quad = \text{VORTAD} + \text{TAD}, \quad (4)$$

where the first term on the right-hand side is the differential vorticity advection term (VORTAD), while the second term indicates the temperature advection influence (TAD).

For diagnostic purposes, the evolution of some atmospheric variables over some key regions will be considered; they are indicated in Fig 1.

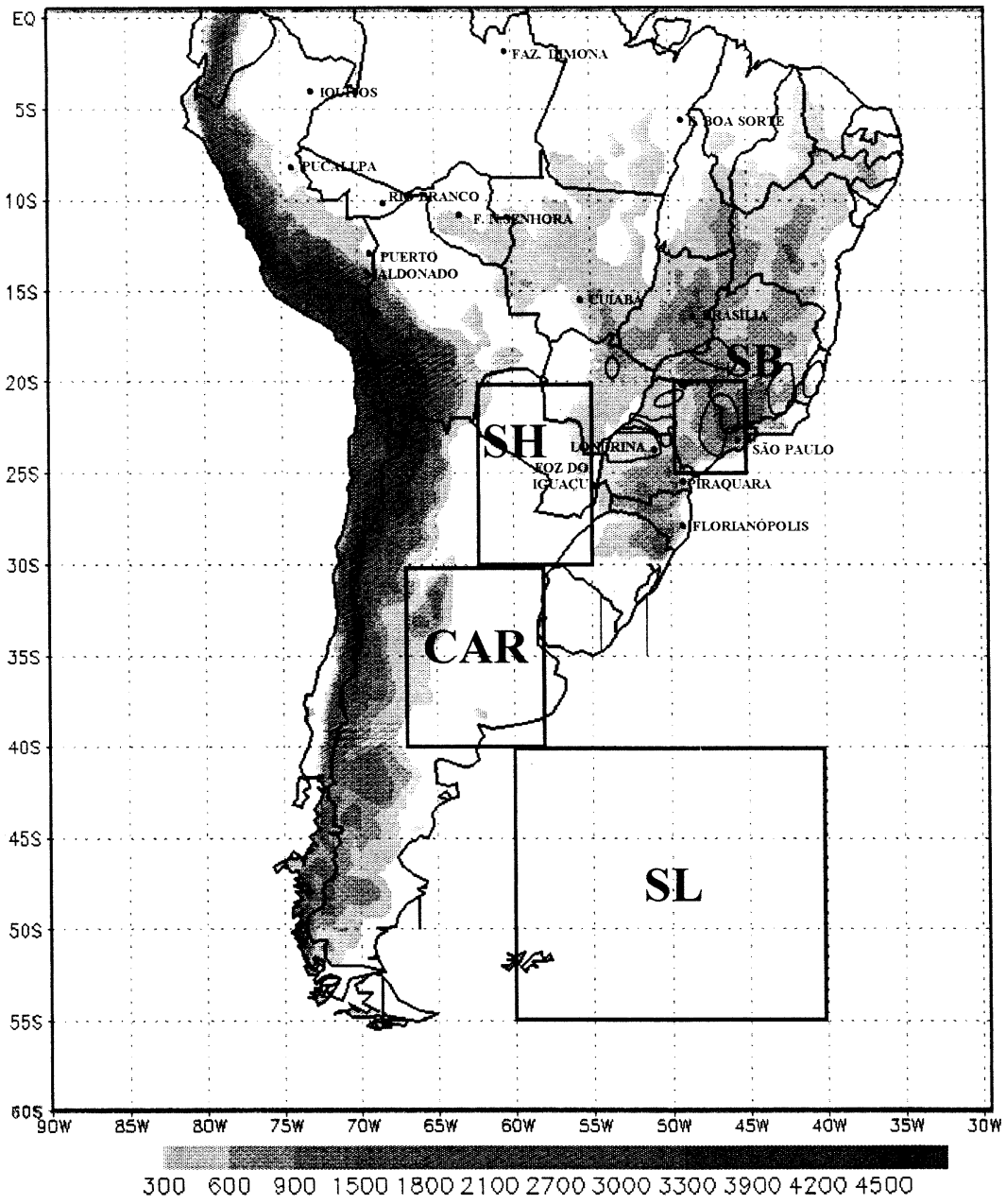

FIG. 1. Terrain map for stations in Brazil and Peru, for which records have been used in the present investigation. Elevation (above 300 MSL) as shown in the gray-scale bar (m). Areas in which coffee is grown in southern Brazil are indicated by solid curves. The areas CAR, SL, SB, and those for which indices have been constructed are shown in rectangles.

3. Cold-air invasions in 1994

According to CPTEC reports, during the 1994 May–August winter season, 14 cold waves, some of them associated with frost and snow, affected southern Brazil. Some of these cold waves moved equatorward and reached southern Amazonia, producing sharp reductions of temperature in southern Amazonia, while the cooling was not so strong over central Amazonia. In the following section we will describe the June cooling episode.

a. Minimum air temperature in the June 1994 case

Figure 2 shows the daily evolution of minimum temperatures during this episode. From this figure, as well as from CPTEC, it follows that during 20–30 June 1994, temperatures below 0°C were registered on 26 June near

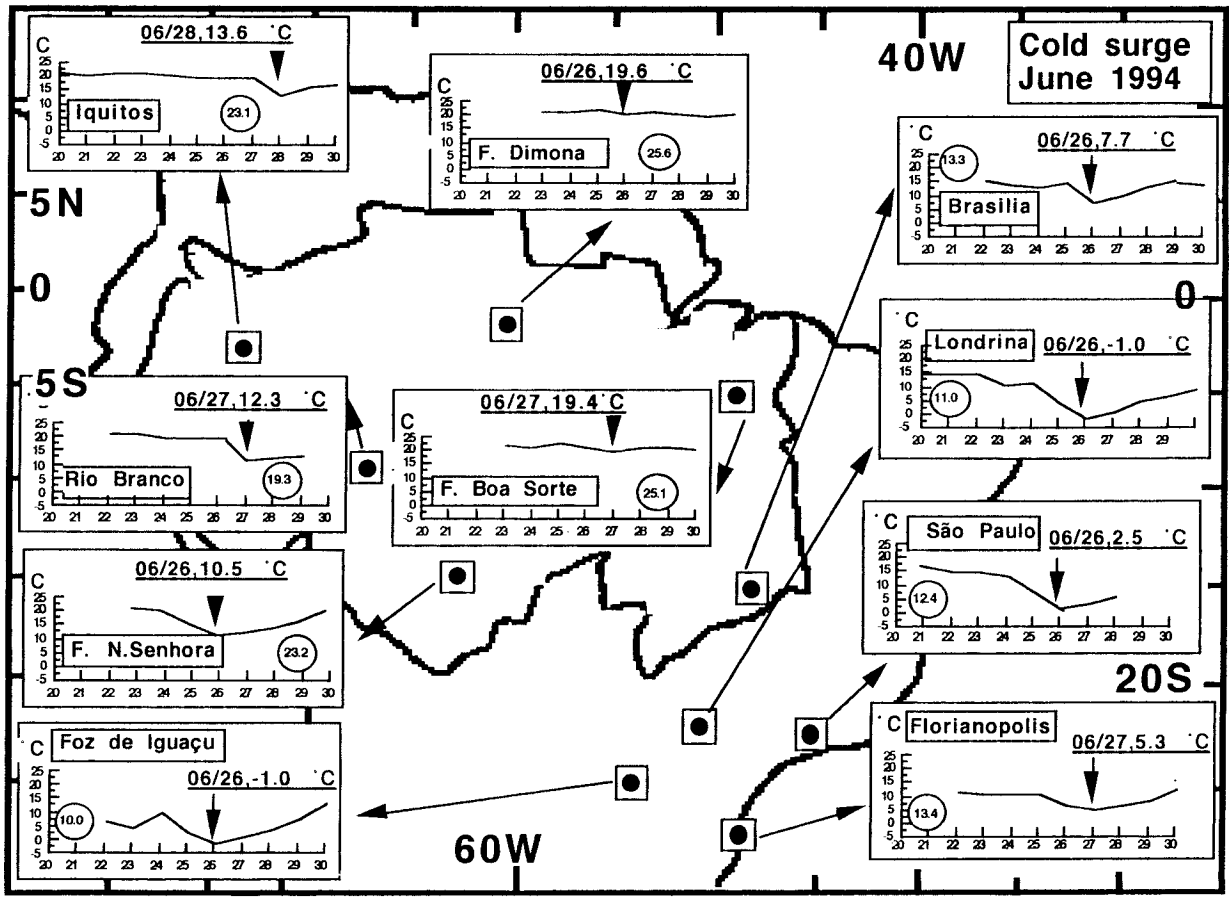

FIG. 2. Cold surge of June 1994. Minimum temperatures (°C) are for the period 20–30 June 1994 in Iquitos (3°45′S, 73°15′W), Rio Branco (09°58′S, 67°48′W), Londrina (23°20′S, 51°08′W), Brasilia (15°47′S, 47°56′W), São Paulo (23°37′S, 46° 39′W), Foz de Iguaçu (25°31′S, 54°35′W), and Florianopolis (27°40′S, 48°33′W). In addition, we used stations from the ABRACOS sites: Fazenda Dimona (2°19′S, 60°19′W), Fazenda Nossa Senhora de Aparecida (10°45′S, 62°22′W), and Fazenda Boa Sorte (5°10′S, 48°45′W). Arrow indicates the day and the temperature of the coldest day. Station locations are indicated by dots inside the rectangle. Long-term mean minimum temperatures of the month are in a circle. Locations are indicated in Fig. 1.

the coffee-growing areas in southeastern Brazil, while less cooling occurred in southern and western Amazonia. In western Amazonia, the minimum temperatures during the coldest days were several degrees cooler than the normal, occurring 1–2 days after the coldest day in southeastern Brazil. Not much cooling was detected in eastern and central Amazonia.

Data from the ABRACOS experiment helped us in identifying the evolution of the cold wave in Amazonia. Air temperatures dropped to a minimum of 10.5°C on 26 June at Fazenda Nossa Senhora (southwestern Amazonia). In northern and eastern Amazonia, the records at Fazendas Dimona and Boa Sorte indicated that the coolest days occurred on 26 and 27 June, respectively; the days were not as cold as in southern Amazonia, indicating a modification of the cold air over equatorial latitudes while it was moving toward the northeast. Based on the lowest minimum temperatures, the cold surge of June was the strongest in 1994, occurring in southeastern Brazil and southern and western Amazonia. Other cold events in July and August 1994 showed similar behavior in southern Amazonia and southeastern Brazil, but were less cold than the one in June (A. Culf 1996, personal communication).

Figures 3a–f show the time evolution of sea level pressure and dewpoint temperature as the cold front passed over stations in the Tropics and in southern Brazil during the cold surge episode of June 1994. The changes in pressure and dewpoint display the obvious frontal signatures associated with cold air mass displacements. The amplitude of these variations are an indicator of the intensity of the phenomenon and, at the same time, the detection of the spatial extent across the Amazon basin and southern Brazil. As expected, the dewpoint and pressure curves show opposite trends during the cold surges.

To identify the presence of the cold front and the cold air mass behind it, Figs. 4a–j show the evolution of the 0900 LT air temperature, wind speed, and direction for two stations in southeastern Brazil (Piraquara and Lon-

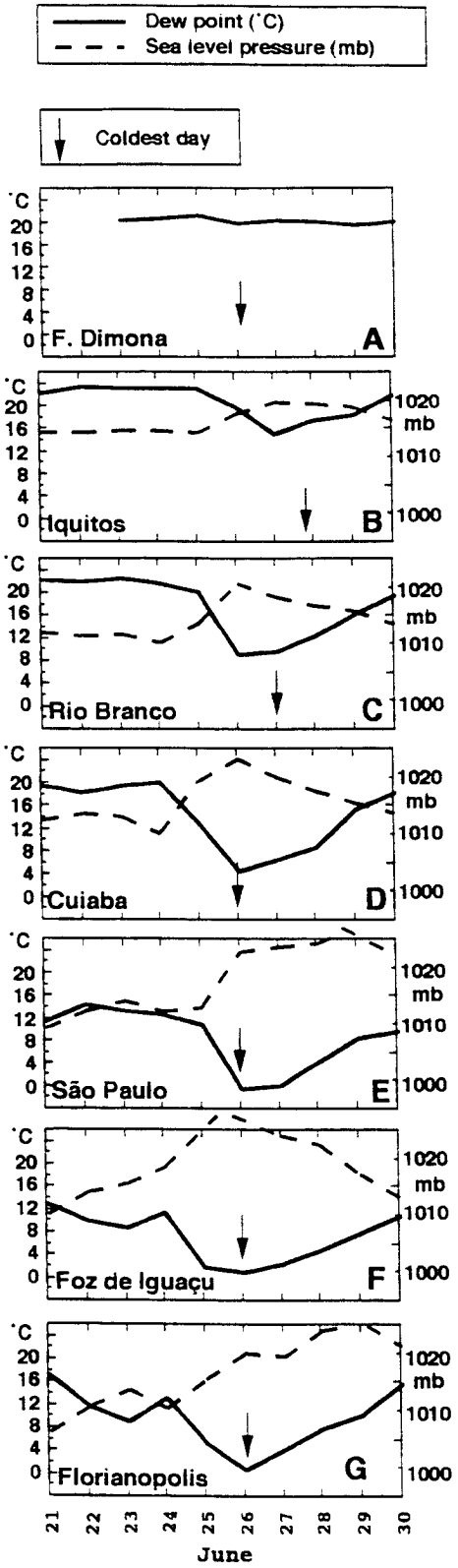

FIG. 3. Sea level pressure (dashed line) and dewpoint temperature (solid line) for 21–30 June [(a)–(g)]. Stations used are located in Amazonia and southern Brazil: (a), (h), for Fazenda Dimona; (b), (i) for Iquitos; (c), (j), for Rio Branco; (d), (k), for Cuiaba; (e), (l), for São Paulo; (f), (m), for Foz de Iguaçu; and (g), (n) for Florianopolis. Sea level pressure data was not available for Fazenda Dimona. For location see Fig. 1 and caption of Fig. 2.

drina; Figs. 4d–e, 4i–j) and three stations across Amazonia (Fazenda Boa Sorte, Fazenda Dimona, Fazenda Nossa Senhora; Figs. 4a–c, 4f–h). The amplitude of the air temperature curve is larger at stations located in southeastern Brazil, compared to northern or central Amazonia, indicating that the cooling is stronger at these sites. As for the wind speed and direction, higher wind speeds are observed before or on the coldest day of 26 June, with a steady component of wind from the south especially noticeable in southern Amazonia (Fig. 4h), Londrina (Fig. 4i), and Piraquara (Fig. 4j).

The temperature contrast, together with the gradient in surface pressure and humidity (from Fig. 3), and the change in the wind speed and direction, all indicate the nature of the two different air masses, allowing for frontal identification. Without the temperature contrast, the front has little or no dynamic significance. The analysis of Figs. 3 and 4 shows that based on those contrasts, the cold front has some significance in southeastern Brazil and southern Amazonia but not in northern and eastern Amazonia.

From the amplitude of the changes in air temperature and wind, the intensity of the cold surge is larger in southern and southeastern Brazil, where changes in pressure quite often exceed 10 hPa and sometimes 15 hPa in 24 h, coincident with changes in dewpoint in the order of 5°–12°C (Figs. 3d–g, 3k–n, 3r–u). The fall in the dew point temperature is fast, taking only 24–48 h, whereas the return to ambient conditions is slow, taking more than 96 h. The lowest dewpoint temperature occurs 48 h after the minimum pressure takes place, that is, the passage of the cold front. Pressure variations associated with the passage of the cold front are less than 5 hPa over two days in Iquitos, while in southern Brazil the changes are greater than 12 hPa in 1 or 2 days. In Foz de Iguacu, pressure dropped 10 hPa between 24 and 26 June. The coldest day, indicated with an arrow, shows a steady equatorward movement of the cold air.

b. Synoptic situation and cloud imagery

In the following section, the surface synoptic features of the cold surges are discussed. As reported by CPTEC, on the third week of June, the atmospheric flow over the South Pacific showed a southwest–northeast orientation of the subtropical jet over South America, associated with a deep trough along the coast of southern Brazil and Argentina, which favored the movement of frontal systems and anticyclones into lower latitudes. This was especially noticeable on 23 June (Fig. 5a), 3 days before the coldest date, and to a lesser degree on 26 June (Fig. 5b, the coldest day). On 23 June, a pair

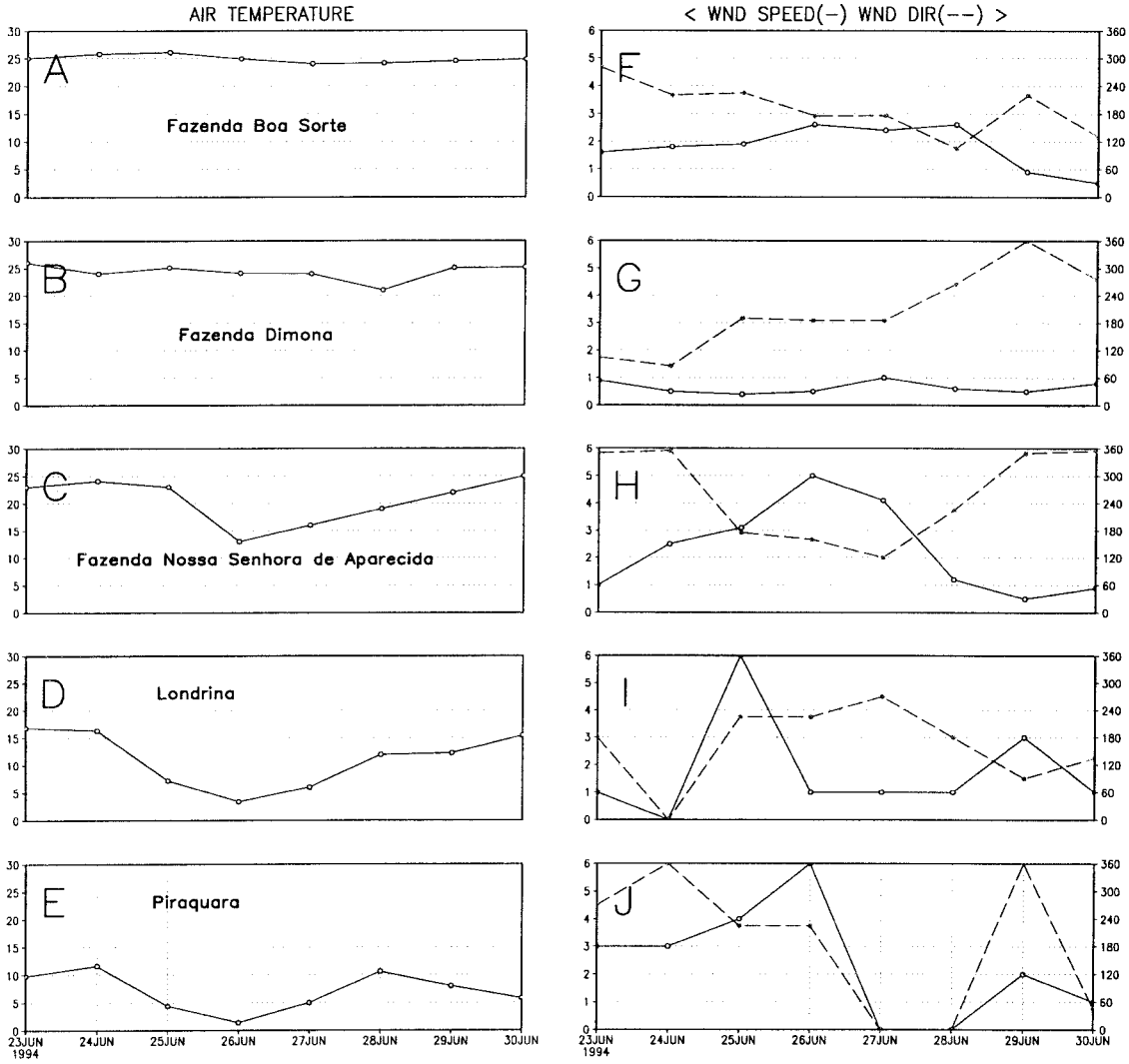

FIG. 4. Air temperature and wind speed and direction during the cold surge of 23 June–1 July 1994 for stations located in a north–south transect from Amazonia to southern Brazil (see Fig. 1). Locations are Fazenda Boa Sorte, Fazenda Dimona, Fazenda Nossa Senhora de Aparecida, Londrina, and Piraquara. The data is for 0900 LT. (a), (f) Fazenda Boa Sorte; (b), (g) Fazenda Dimona; (c), (g) Fazenda Nossa Senhora de Aparecida; (d), (i) Londrina; and (e), (j) Piraquara.

of ridge–trough systems were detected over the central and eastern Pacific, traveling eastward, with a deep trough over the coast of southern Brazil and Argentina. On this day, the trough showed a strong confluence over northern Argentina of flow from the southwest and the northwest. On 26 June those systems moved to the east, with one ridge parallel to the coast of Chile and the trough still deep over southern Brazil and north-central Argentina.

A sequence of surface charts (Figs. 6a–l) are shown from 1200 UTC 23 June to 1200 UTC June 27. The maps are shown every 12 h, with a smaller interval (6 h) for the period when the cold-core anticyclone enters South America, so the details and the behavior of the surface synoptic fields can be better appreciated. Cloud imagery from the GOES satellite are shown in Figs. 7a–f, helping to clarify the extent of the cloudiness associated with the cold front and the lack of cloudiness associated with anticyclonic conditions. The figures include overlays added to identify the positions of the cold-core anticyclone (H), the low pressure systems in the southern Atlantic (L), and the cold front. The position of these systems is from the appropriate 1200 UTC NCAR–NCEP reanalyses at the surface.

At 1200 UTC 23 June (Fig. 6a) the anticyclone was located at approximately 35°S, 92°W, and there were two troughs: one over southern Argentina and the other near the coast of Argentina and Uruguay along 45°W. The GOES image (Fig. 7a) shows cloudiness above the two trough areas. The trough over Argentina was marked by low stratiform cloud cover over the adjacent ocean areas. Scattered cloudiness was observed over

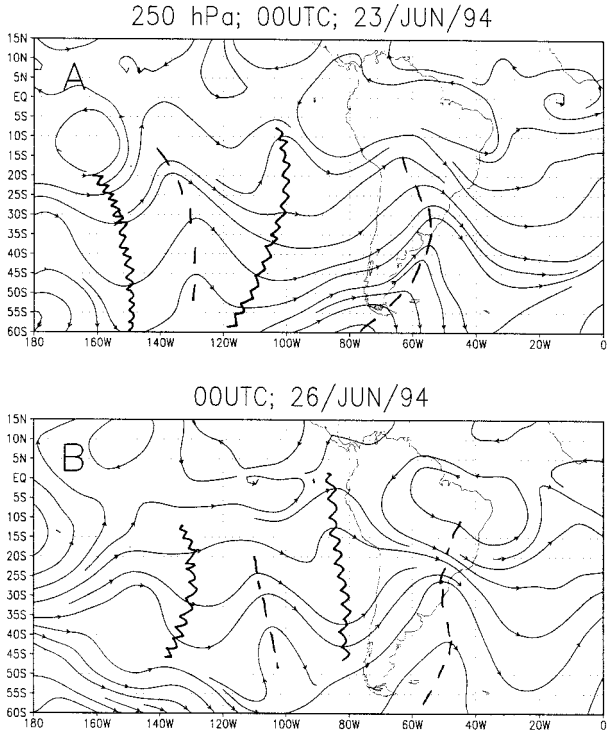

FIG. 5. At 0000 UTC for 250-hPa circulation (a) 23 June 1994 and (b) 26 June 1994. Troughs and ridges are indicated on the flow maps.

southern and central Amazonia. Figure 6b shows that, in the following days, the first trough evolved into a cold front and its related cyclone intensified and moved to the east.

At 0000 UTC 24 June (Fig. 6b) the anticyclone over the Pacific moved to the east, reaching 85°W, while at 1200 UTC on the same day (Fig. 6c) the anticyclone intensified and was located closer to the coast of South America. The trough evolved into a cold front that extended over the extreme southern Brazil, and the cyclone was more intense and now located over 42°S, 53°W. The GOES image at 1200 UTC (Fig. 7b) shows that the cold front and associated cloud band moved northeastward and was now placed over southern Brazil. Clear skies were found over southern and eastern Amazonia.

Starting at this time, the anticyclone approached the Andes, and the curvature of the isobars south of 40°S indicated that the cold air was trying to cross the Andes where elevation is lower (Figs. 6c–i). This was observed from 1200 UTC 24 June (Fig. 6c) through 0600 UTC 25 June (Fig. 6f). In this period, the front was located in southeastern Brazil, and the cyclone over the south Atlantic became more intense and eastward displaced. With respect to the anticyclone passing the Andes, Lichtenstein (1989) indicated that cold air that enters the continent from the southeast, where elevation is more than 2000 m MSL, cannot cross the Andes and so is forced to turn around the obstacle, increasing its anticyclonic curvature. This can be observed south of 45°S in Figs. 6c–f.

From 1200 to 1800 UTC 25 June (Figs. 6g and h), the anticyclone moved along the east flank of the Andes with an intensity of 1030 hPa, while the cyclone over the south Atlantic reached 980 hPa and the cold front was located over Rio de Janeiro. Cloud imagery (Fig. 7c) shows the cold front and cloud band extended from the south Atlantic to western Amazonia, while central Amazonia was under clear conditions. Clear skies behind the cold front over southern Brazil and Uruguay indicate low temperatures for those regions

On the coldest day, 26 June, the maps at 0000 and 1200 UTC (Figs. 6i, j) show that the anticyclone was located over southern Brazil, extending into southwestern Amazonia, even though it was somewhat reduced in intensity (1025 hPa). The cold front was now over southeastern Brazil, reaching eastern Brazil 12 h after. Concomitantly, the cold front and related cloud band (Fig. 7d) moved to the northeast, with some cloudiness over central and eastern Amazonia, while southern Amazonia was under clear conditions. Clearing behind the front led to a dramatic change in surface temperatures in southeastern Brazil. On this day temperatures of less than 0°C were recorded at Londrina and Foz de Iguacu (Figs. 1 and 3).

At 0000 UTC 27 June (Fig. 6k) the anticyclone weakened (1020 hPa), and by 1200 UTC (Fig. 6l) it had moved to the east. At 1200 UTC (Fig. 7e) the cold front and cloud band were located over eastern Brazil. Subsequently, the anticyclone reached the south Atlantic. At 1200 UTC on 28 June (Fig. 7f) central Amazonia appeared to be covered by midlevel clouds or shallow fair-weather cumulus. In this period, the cyclone intensified, reaching 970 hPa (20 hPa lower than on 23 June), and was located at 50°S, 40°W.

c. Critical comparison of this case with two others of the winter of 1994. How different is it from a typical situation?

The 26 June event, as well as other events like 9–10 July and 10 August 1994 (not shown here) are characterized by the presence of an anticyclonic perturbation off the coast of Chile that enters South America and turns around across the Andes south of 45°S, where the elevation is relatively low. The northward displacement of the anticyclone followed a meridional continental track until reaching around 20°–30°S, then moving eastward toward the Atlantic. This is a typical feature in these three cases, as well as in other cases documented in the literature. The difference could lie in the intensity of the northward flow along the east flank of the Andes, in the intensity of the high pressure, and in the latitudinal positions of both the entrance of the anticyclone into South America and its most equatorial position during the coldest days. The area affected by the anticyclone also varies, especially in the southeast flank.

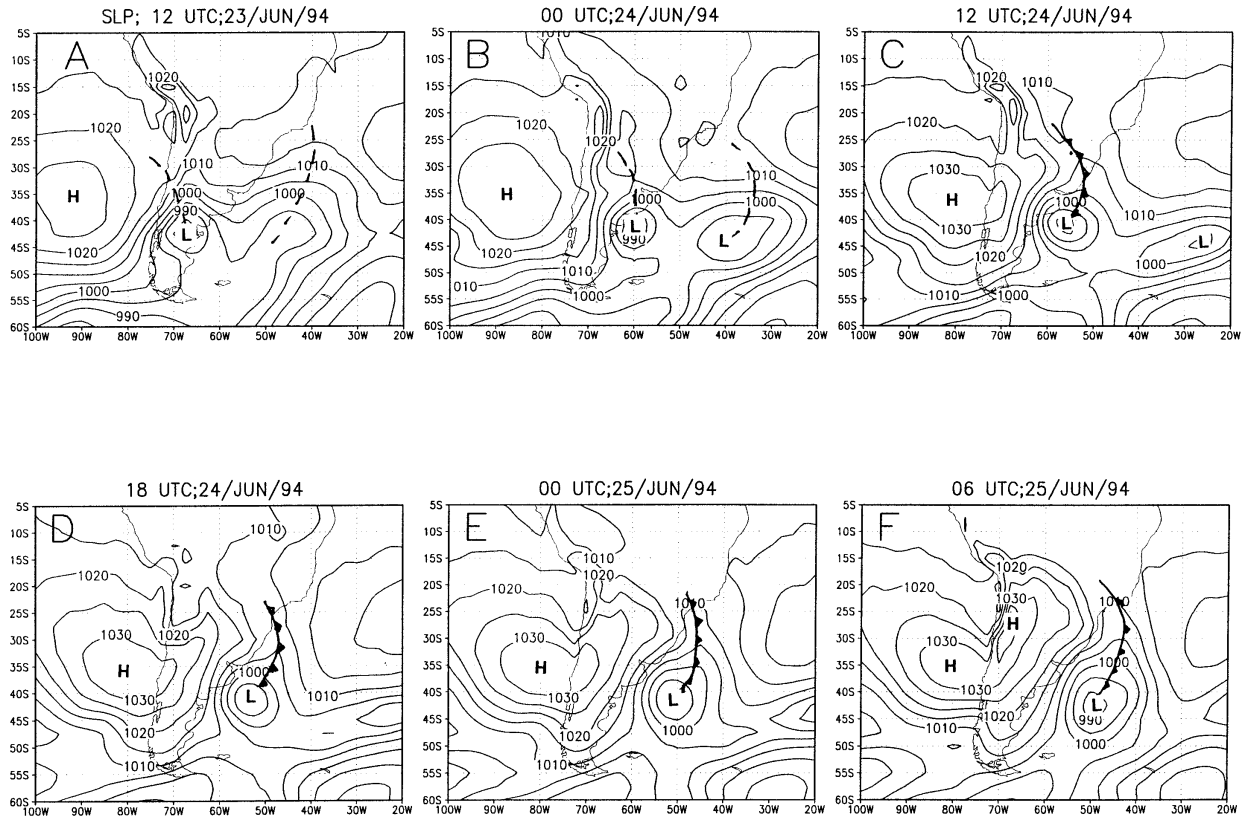

FIG. 6. Surface weather conditions (sea level) from 1200 UTC 23 June to 1200 UTC 27 June 1994. Troughs, fronts, and the position of the high (H) and low (L) pressure centers are indicated on each map. (a) 1200 UTC 23 June, (b) 0000 UTC 24 June, (c) 1200 UTC 24 June, (d) 1800 UTC 24 June, (e) 0000 UTC 25 June, (f) 0600 UTC 25 June, (g) 0200 UTC 25 June, (h) 1800 UTC 25 June, (i) 0000 UTC 26 June, (j) 1200 UTC 26 June, (k) 0000 UTC 27 June, and (l) 1200 UTC 27 June. The surface weather maps are plotted from the NCEP–NCAR reanalysis.

From the analysis of minimum temperatures, dewpoint, and surface pressure, the amplitude of the changes is different for each location and different at the same place for each case (as compared to July and August 1994 cases). These changes have the same tendency but different magnitudes, which indicates that in all cases the cold surges show the same basic characteristics, but each is different with respect to the degree of cooling produced.

At this stage, one could ask: If the cold events follow the same pattern and basically they seem similar initially, why do some particular episodes bring the cold air more equatorward, while many others do not? What forces the cold air to move northward and reach Amazonia with different intensity? Is there any large-scale dynamical influence and/or an interaction with the Andes that triggers this phenomenon? These questions will be answered in the following section.

4. Dynamic analysis and diagnosis

We consider two steps in the evolution of the event: the starting and the developing periods. In the first step, some characteristic perturbation is detected when it shows up near central and southern Chile in the Pacific Ocean. During the developing period, several processes take place in southern South America conducive to the presence of low minimum temperatures over southeastern Brazil. In the following sections, unless we explicitly indicate otherwise, we will be referring to the cold event in which the coldest day in southern Brazil occurred on 26 June 1994.

a. Starting period

1) LOW SEA LEVEL PRESSURE

Figures 8a and 8b show the sea level pressure (SLP) revolution (Hovmoeller diagram) at 45°S related to 300-hPa cyclonic (negative in the Southern Hemisphere), vorticity advection (CVA), and 600-hPa upward vertical velocity (UVV). Figure 8a suggests that the SLP in this phase may have been associated with CVA from an upper-level trough approaching the continent from the Pacific (Fig. 9), as shaded areas indicate the presence of CVA and UVV (Figs. 8a, b) corresponding to SLP drops. Figure 8b also shows that a 300-hPa cyclonic intensification took place west of the Andes from 22 to

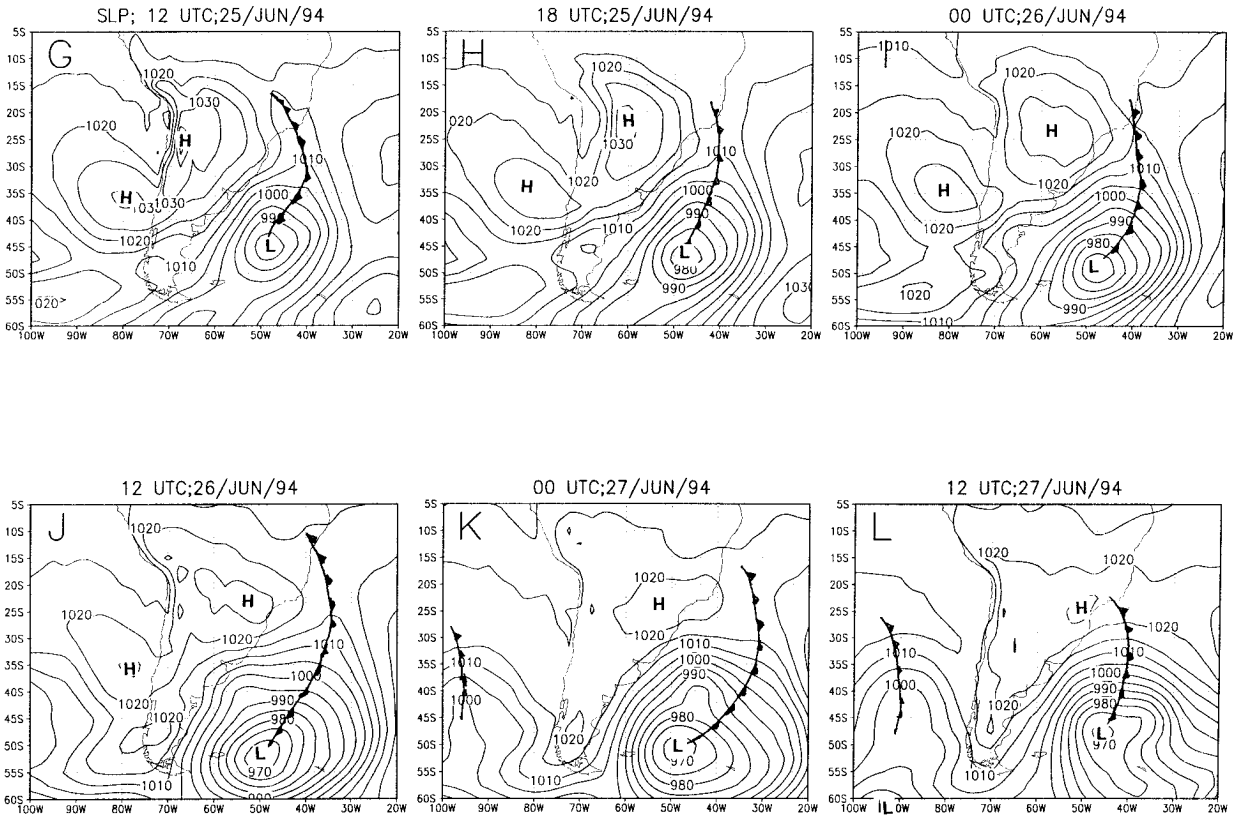

FIG. 6. (*Continued*)

23 June, corresponding to a trough reaching near the Andean longitudes on about those days (Fig. 9b).

Notice in Fig. 8a that east of the Andes, near the 65°W longitude, a low SLP contour of 994 hPa was present at about 1200 UTC 23 June (hereafter 12/23). Figure 8c shows that the SLP low (shaded) was located ahead of the upper-level trough moving into the continent. Significant CVA would promote upward motions with low-level convergence and SLP drops.

Notice also in Fig. 8a that during and after the largest SLP drop, strong SLP gradients remained intense east of the cordillera from 12/23 to at least 12/24, due to the fact that the upper-level trough moved relatively slowly. These significant zonal SLP gradients allowed for equatorward cold-air transport produced by the associated southerly winds channeled by the Andes.

From another perspective, Figs. 9a, b show the eastward displacement of the 500-hPa trough in the southeastern Pacific toward the continent. Notice that as it reached the Andes on about 12/23, the trough intensified as the relative vorticity developed more negative values. During the following day, the trough kept its intensity, but another deepening took place when it reached near eastern Brazil longitudes (Fig. 9d).

2) LOW-TROPOSPHERIC TROUGHING

In this section we will consider the levels below those corresponding to the maximum vertical velocity, which usually occurs at about 600 hPa. Perhaps one of the most important features in the starting period is the low-tropospheric trough that deepens near the Andes in association with the intensification of the 500-hPa trough in the same area (Fig. 9).

In Fig. 10a, we present a Hovmoeller diagram of the 700-hPa absolute vorticity (ABSVOR), as it was diagnosed by NCEP–NCAR, related to the negative values of DIVTERM (shaded) in the vorticity equation [Eq. (2)]. Notice that windward of the Andes (west of about 75°W) during the period 12/22–00/23, ABSVOR decreased (cyclonic intensification) associated with the presence of negative values of DIVTERM in the vorticity equation. This feature indicates that the UVV that were discussed in section 5a(1) were also very important in the local intensification of the low-level trough near the Andes. To understand this fact further, we present in Figs. 10b–e the corresponding vorticity equation terms [Eq. (2)] for a day in which local cyclonic intensification was occurring. Figures 10b, c suggest that the equation is a reasonable approximation as most of the observed main features are explained by HVOAD and DIVTERM and that, in general, both terms were of similar importance as Figs. 10d, e suggest. The latter term is produced by column stretching due to upward velocities. The most notable feature in Fig. 10b is the local intensification of the 700-hPa trough leeward of

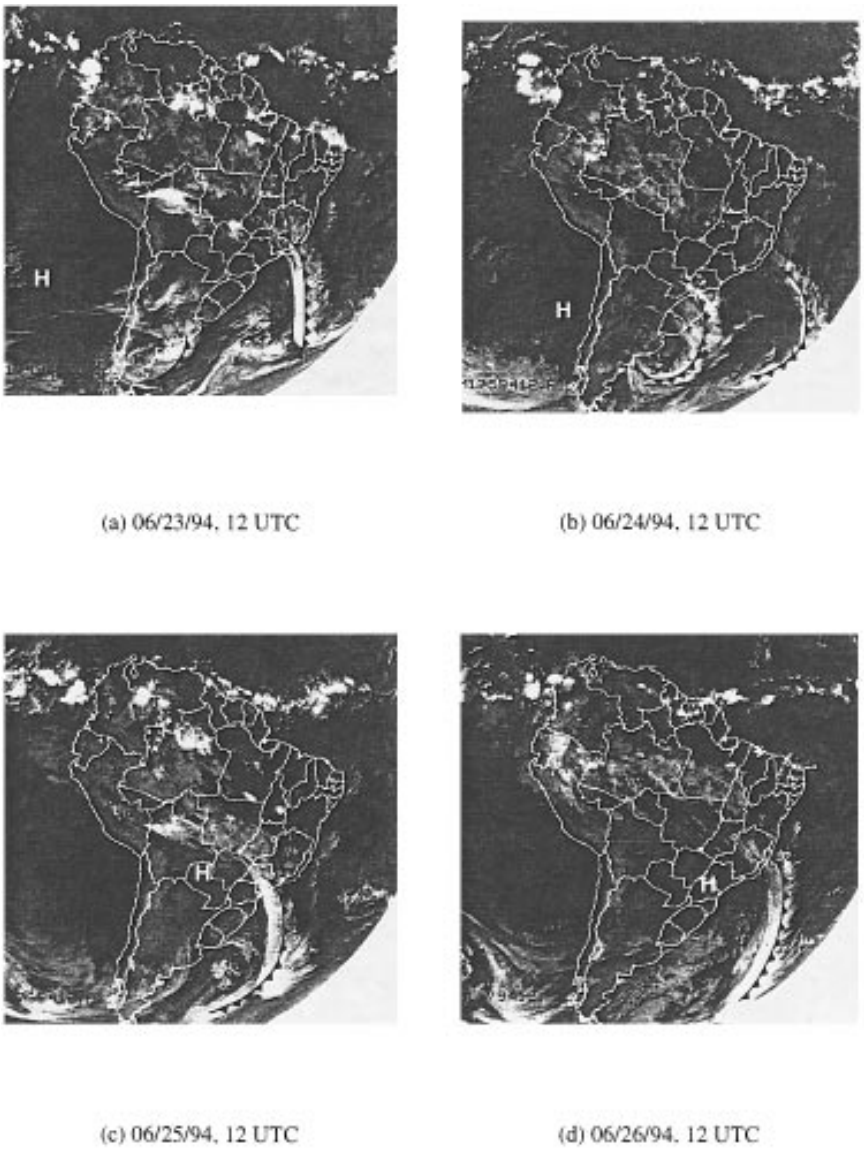

FIG. 7. Series of *GOES-8* enhanced IR images, 1200 UTC for (a) 23 June, (b) 24 June, (c), 25 June, (d) 26 June, (e) 27 June, and (f) 28 June. Surface features such as the cold front and the anticyclone (H) are from NCAR–NCEP reanalysis from 1200 UTC.

the Andes in the 35°–50°S range due to contributions from both HVOAD and DIVTERM. Figure 10a shows that DIVTERM was present while the trough was deepening, suggesting that it was a persistent contributor.

We may also notice in Fig. 10a that on 12/23, an ABSVOR minimum of about -16×10^{-5} s^{-1} was present near 67.5°W. Later this trough weakened as it kept moving eastward, reaching 55°W on 12/24. As in the SLP low case, this 700-hPa trough remained intense for several days east of the Andes, from 12/23 to at least 12/24 (Fig. 10a), which may have kept substantial height gradients east of the Andes at least on 24 June. The associated southerlies between the trough and the cordillera may have produced equatorward cold-air transports channeled by the Andes. From another perspective, Fig. 11 presents the 700-hPa relative vorticity field for several instances previous to the starting phase. The intensification of the trough when crossing the Andes is apparent.

In summary, the vorticity balance analysis shows that at 700 hPa during the starting period, a trough locally intensified leeward of the Andes near 40°S due to contributions from HVOAD and DIVTERM (Fig. 10b).

3) INITIAL COOLING

Figure 12a shows the 700-hPa temperature evolution (Hovmoeller diagram) at 42.5°S, related to the negative

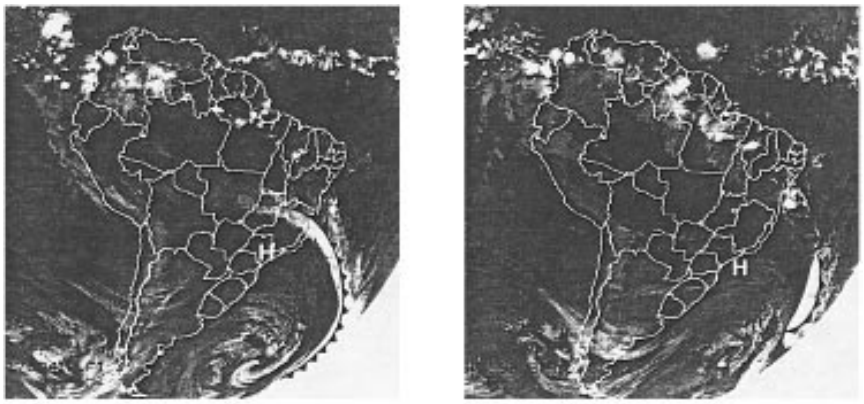

(e) 06/27/94, 12 UTC (f) 06/28/94, 12 UTC

FIG. 7. (*Continued*)

values of HTADV (shaded) in the thermodynamic equation [Eq. (1)]. Notice that strong temperature drops were present simultaneously with large HTADV values. Notice also that the cooling took place west of the Andes during the period 00/23–12/23, when the trough obtained its maximum local intensification in the same region (Fig. 10b), suggesting that the associated southerlies, west of the trough, were responsible for the cold advection. The same conclusion may be obtained comparing Figs. 12c and 12d, where cold advection west of the Andes was due to southerlies associated with a deepening trough.

To emphasize this relationship further, we show in Fig. 13 the thermodynamic equation [Eq. (1)] terms corresponding to a day in the starting period. Figure 13a presents the local temperature change (left-hand side), while Fig. 13b shows the sum of the three right-hand-side terms. The HTADV and (ADIAB + WADV) fields

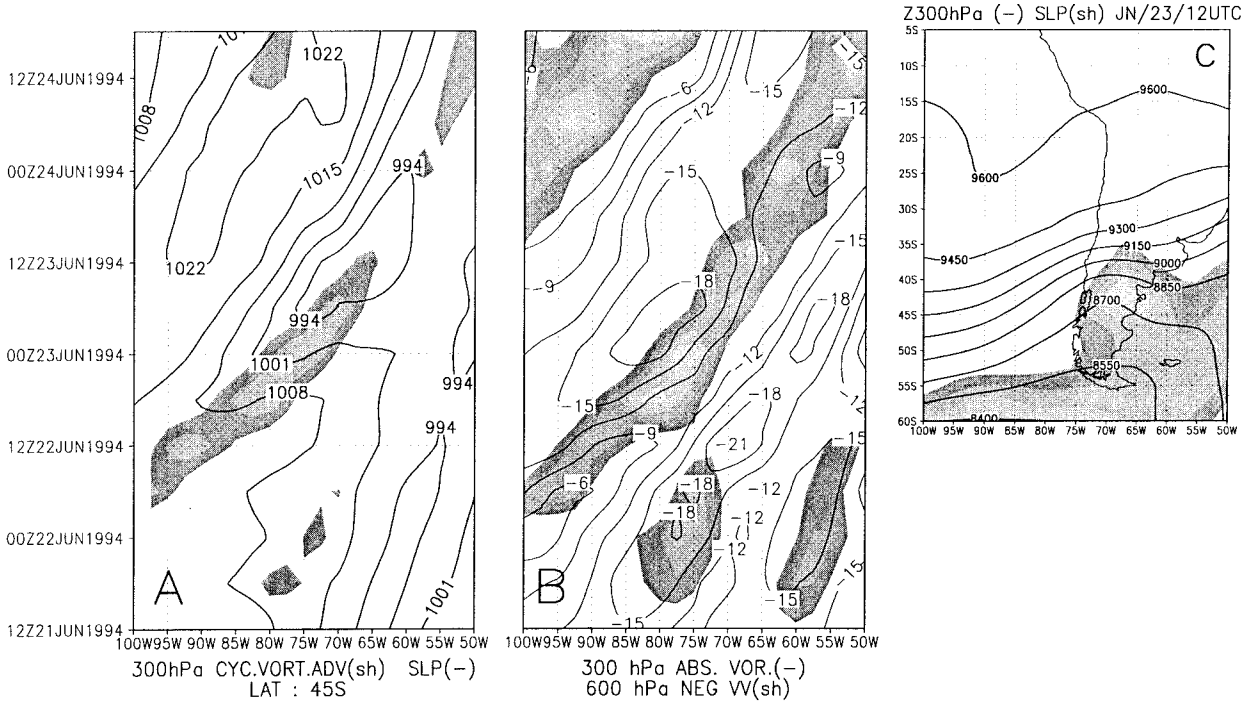

FIG. 8. (a) Evolution (Hovmoeller diagram) of SLP at 45°S (hPa interval is 7 hPa). Shaded areas represent 300-hPa cyclonic vorticity advection (CVA). (b) The 300-hPa absolute vorticity (ABSVOR) evolution at 45°S (10^{-5} s^{-1}, intervals 3×10^{-5} s^{-1}). Shaded areas represent upward vertical velocities at 600 hPa. (c) 300-hPa geopotential height (m, interval 150 m). Shaded areas represent SLP below 1005 hPa.

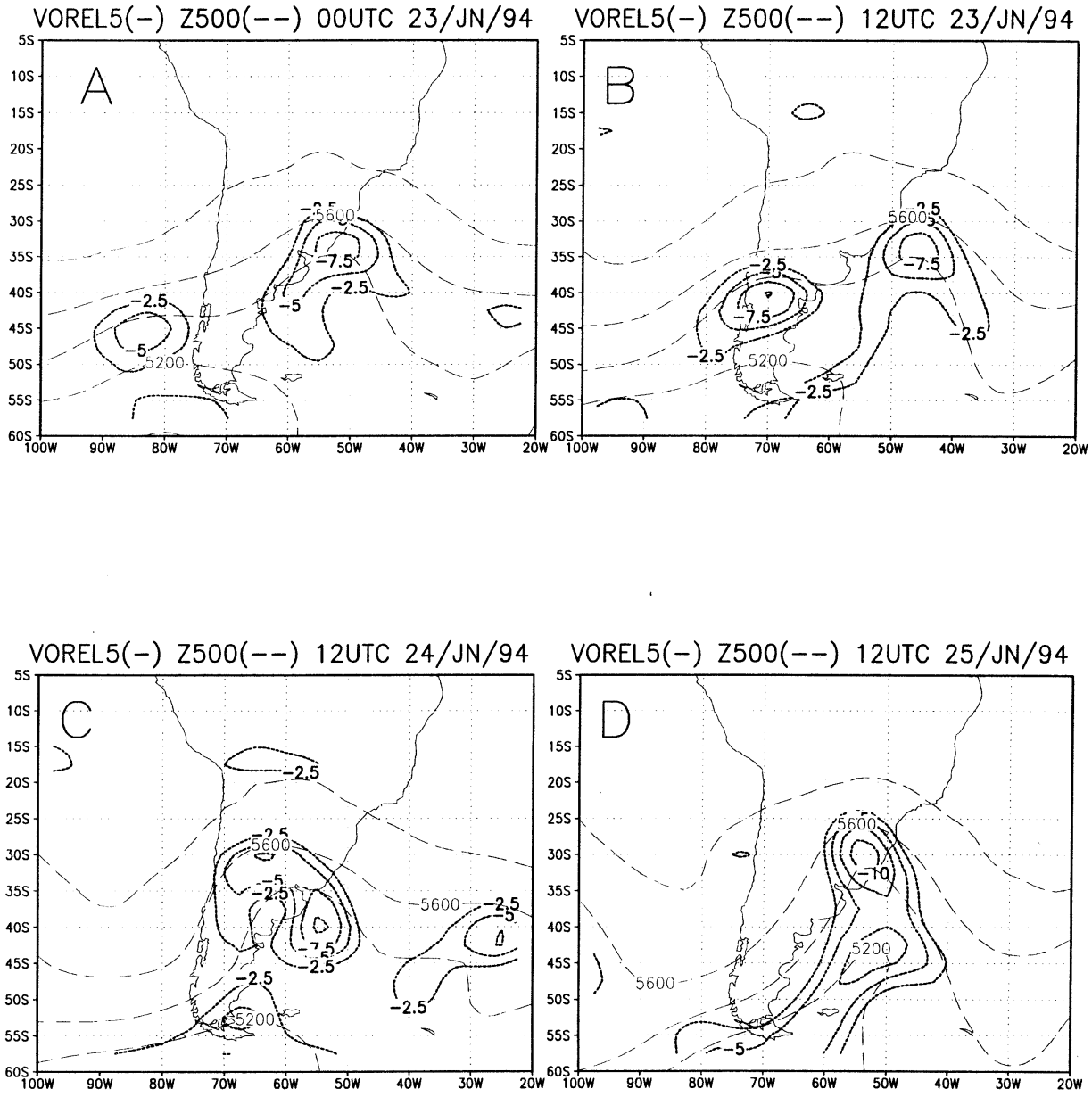

FIG. 9. (a)–(d): 500-hPa cyclonic relative vorticity (10^{-5} s^{-1}, interval 2.5 × 10^{-5} s^{-1}), 500-hPa height (dash, m, interval 200 m).

are shown in Figs. 13c and 13d, respectively. Quantitatively, Figs. 13a, b indicate that in at least the starting period the heating mechanisms considered in the right-hand side explain most of the main features in the observed local temperature change field. Most important, these figures indicate a cooling region centered near 40°S, 75°W where HTADV was dominant.

In Fig. 12b, we present the Hovmoeller diagram (time versus latitude) of the 700-hPa temperature at 62.5°W, just east of the mountains related to the HTADV (shaded) term in the thermodynamic equation. Notice that during the period 18/23 to at least 12/24 there was an equatorward cooling transport. Our results suggest that such cooling was associated with cold advection produced by southerlies west of the locally intensifying 700-hPa trough near the Andes [see section 5a(2)]. It started at 00/23 west of the mountains and later propagated equatorward east of the Andes, reaching near 25°S at 12/24 (Figs. 12a, b).

To emphasize further the different processes in this stage, we will define several indices. They all refer to an area we call CAR (central Argentina) located leeward of the Andes (Fig. 1), where the cooling and troughing mostly take place during the starting period. In previous sections we have seen that the presence of low-tropospheric cold-air advection east of the Andes during the

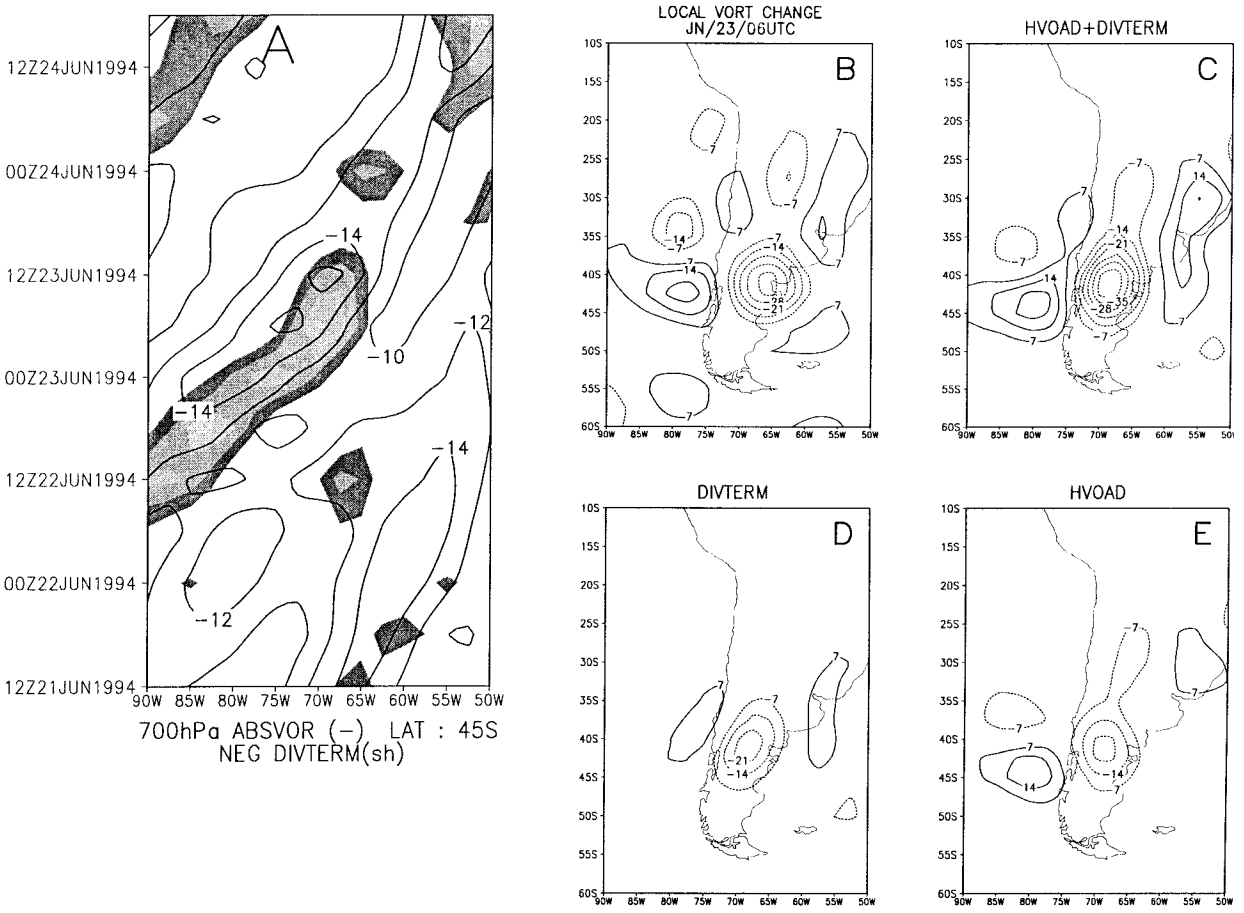

FIG. 10. (a) Evolution (Hovmoeller diagram) of 700-hPa absolute vorticity (ABSVOR) at 45°S (10^{-5} s^{-1}, interval 2×10^{-5} s^{-1}); shaded areas represent negative DIVTERM. (b) Local vorticity change (10^{-10} s^{-2}). (c) Horizontal advection term (HVOAD) plus divergence term (DIVTERM). (d) DIVTERM. (e) HVOAD (10^{-10} s^{-2}).

starting period was a characteristic feature. To get an indicator for this process, an index called TAD7CAR was defined as the average 700-hPa temperature advection over the CAR area. In Fig. 14a, notice that during the periods 12/20–00/23 and 18/23–00/25 such an index remained negative, indicating that cold air was being advected to the area. Consequently, the average 500-hPa geopotential height in the same area, called Z5CAR index, dropped during the same periods, which is an indication that an upper-level trough was locally intensifying east of the Andes at those latitudes.

We would also like to point out another feature when comparing Figs. 12c and 12d. Notice that, due to the cooling process, the temperature gradients had increased in the 30°–40°S range. Additionally, eastward and westward of the cooling zone, stronger zonal temperature gradients were being established, which may have led to the production of eastward cold-air transport during the subsequent days. To quantify this feature we defined the GRT7CAR index as the average square of the absolute value of the temperature gradient in the CAR area. In Fig. 14b, the time series of the TAD7CAR and GRT7CAR indices indicates that the cold advection during the periods centered on 00/22 and 00/24 was associated with increasing GRT7CAR values.

Thus, our results suggest that during the starting period an approaching upper-level trough in midlatitudes intensified when crossing the Andes, producing SLP drops and troughing at least at levels below the maximum upward vertical velocity level. The associated southerlies channeled by the Andes may have produced equatorward cold-air transport. As a result of these processes, significant temperature drops were produced near the Andes, increasing the temperature gradients near the cooling region.

4) A PROPOSED MECHANISM FOR THE STARTING PHASE

In previous sections we have presented evidence of the influence of the upper-level flow pattern (CVA forcing) on the geopotential height time changes at lower levels through the associated ascent. In Fig. 15b, a Hovmoeller diagram (time vs longitude) of the 500-hPa

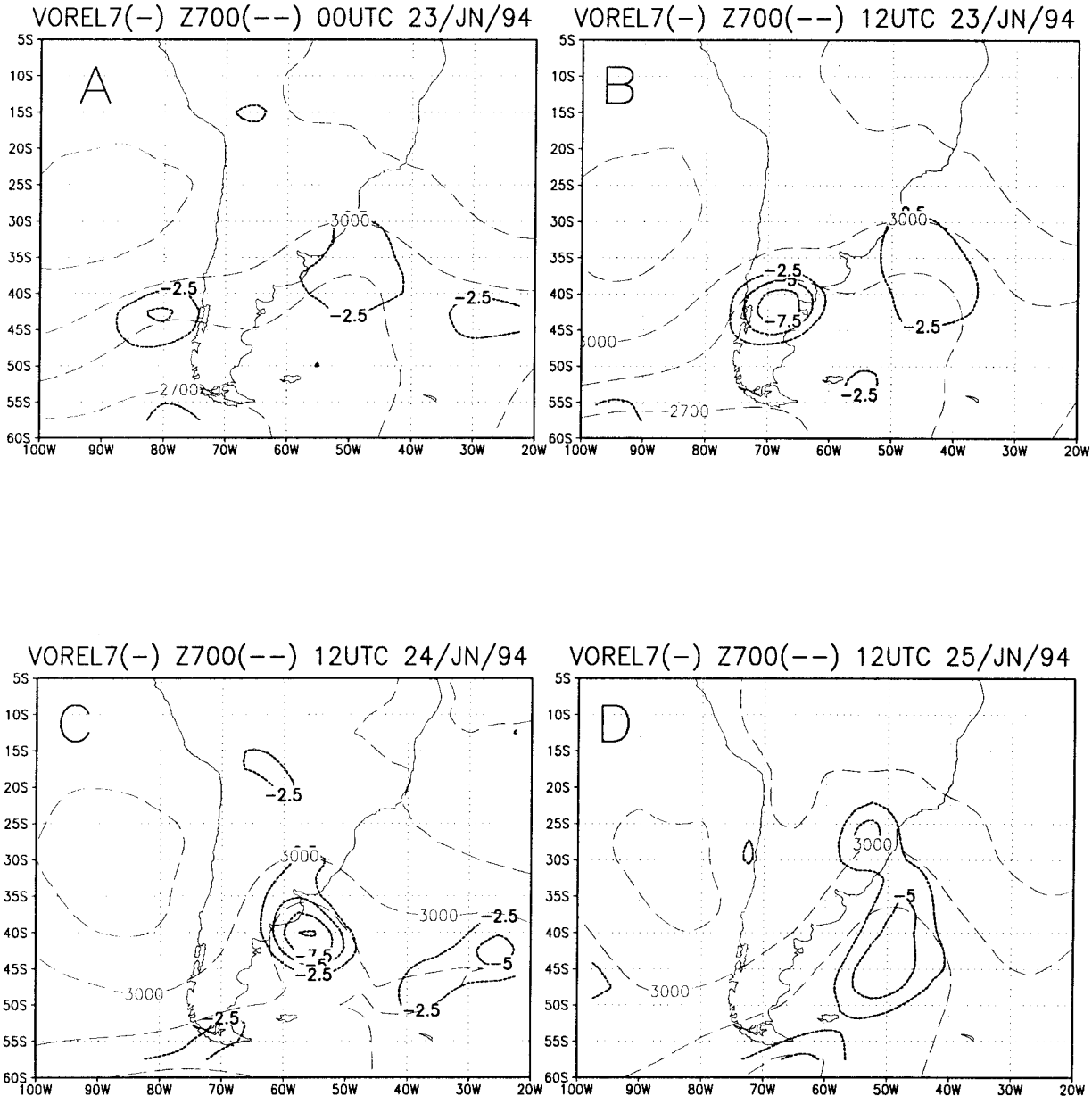

FIG. 11. Same as Fig. 10, but at 700 hPa.

CVA at 35°S related to the evolution of 700-hPa heights confirms the hypothesis; for example, substantial upper CVA signals are associated with low-level height falls mainly during the periods about 22 and 24 June. The same can be said by observing Fig. 15d, where the 700-hPa height falls are shown to be produced ahead of the 500-hPa trough axis in a coherent location with the hypothesis.

On the other hand, Fig. 15a, which shows the Hovmoeller diagram (time vs longitude) of the 500-hPa height related to the C term in the tendency equation [Eq. (3)] indicates that on about 18/23 substantial upper-level height drops were associated with positive C values underneath. As these values are mostly due to low-level cold advection in the region (not shown), it may be concluded that this latter feature (cold advection) may be partially responsible for the upper local troughing by contributing descending motions and the associated convergence and cyclonic time changes at higher levels. The other important contribution to the upper height time changes came from the vorticity advection [B term in Eq. (3)]. In a spatial domain, Fig. 15c presents the same mechanism, that is, the 500-hPa height falls associated with positive C values in a region lee of the Andes.

Furthermore, the 700-hPa height falls in Fig. 15d

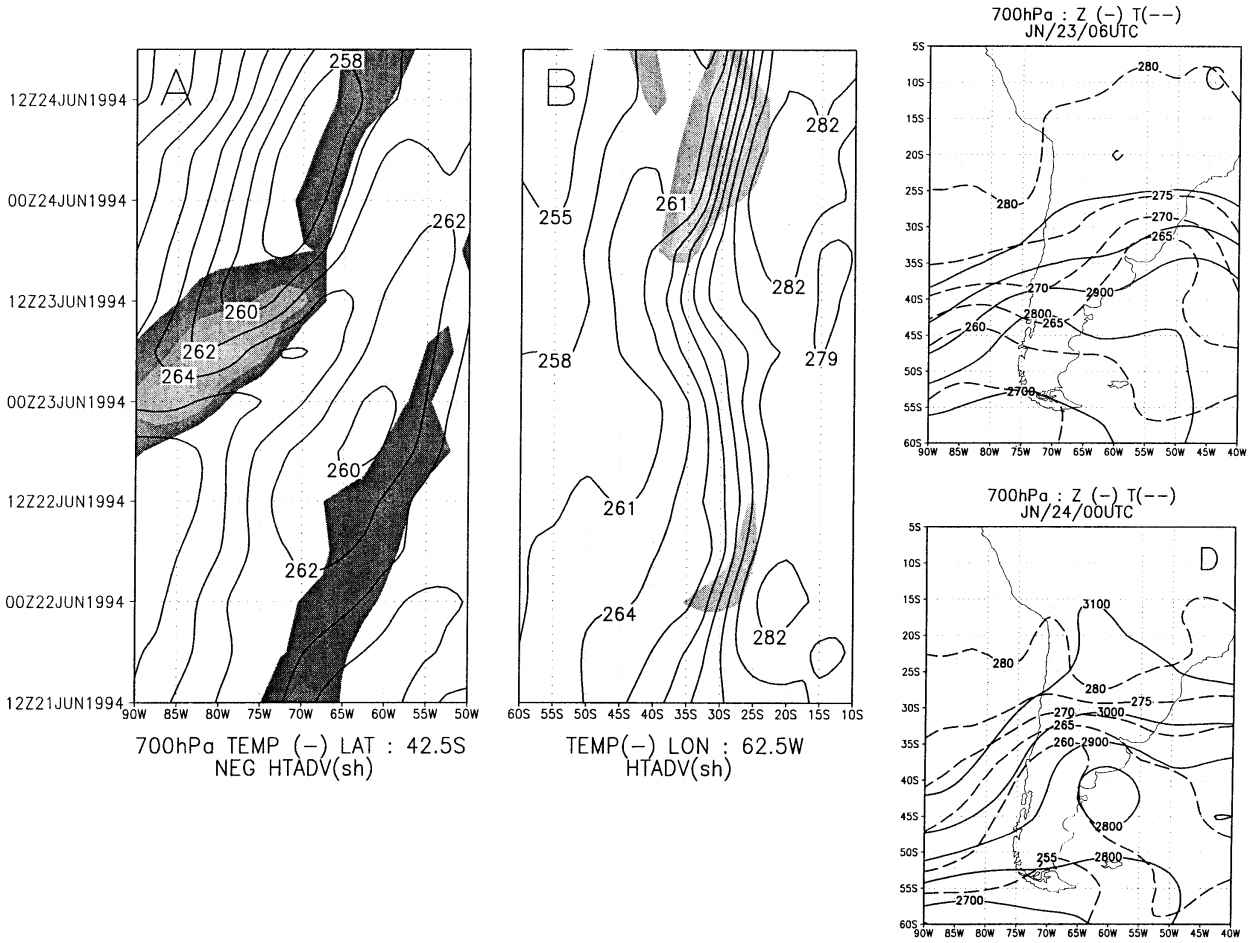

FIG. 12. (a) Evolution (Hovmoeller diagram, time vs longitude) of 700-hPa temperature at 42.5°S (K, interval 2 K). Shaded areas represent negative values of horizontal temperature advection (HTADV). (b) Evolution (Hovmoeller diagram, time vs latitude) of 700-hPa temperature at 62.5°W (K, interval 3 K). Shaded areas represent HTADV heating. (c) and (d) 700-hPa geopotential height (solid, m, interval 100 m) and temperature (dashed, K, interval 5 K).

would make possible the presence of southerlies in a region lee of the Andes and very close underneath the 500-hPa trough axis, which would let northward transport of cold air from higher latitudes, allowing the presence of positive C values (Fig. 15c).

In summary, the evidence presented suggests that local upper-level troughing in the east of the Andes may be partially explained by low-tropospheric cold advection underneath. Other influence is the vorticity advection at those levels [B term in Eq. (3)]. On the other hand, such cold advection would be produced by low-tropospheric local height falls associated with upper-level CVA signals of the intensifying trough. In other words, the low-level flow pattern with the corresponding thermal field would partially drive time changes at higher levels, while in return the latter field would affect the former through the presence of flow time changes. We propose that these processes conform the two parts of a positive feedback mechanism in which the low-level cyclonic tendency is driven by the upper trough intensity, while the latter is influenced by the former through the intensification in low-level cold advection in association with height falls. Notice in Figs. 15c, d that the different features in this scenario are located in coherent locations, that is, the 700-hPa height falls occurring ahead of the upper trough axis in such a location to produce a positive C values region (behind, right under the upper trough axis) in order to be able to contribute to the local intensification of such trough.

b. Developing period

1) UPPER-LEVEL RIDGE AND TROUGH

In a previous section [5a(3)], it was shown that after the east of the Andes cooling, an intensification of the low-level zonal temperature gradients east and west of the cooling area (Fig. 12d) would let cold and warm air advection be produced respectively in those

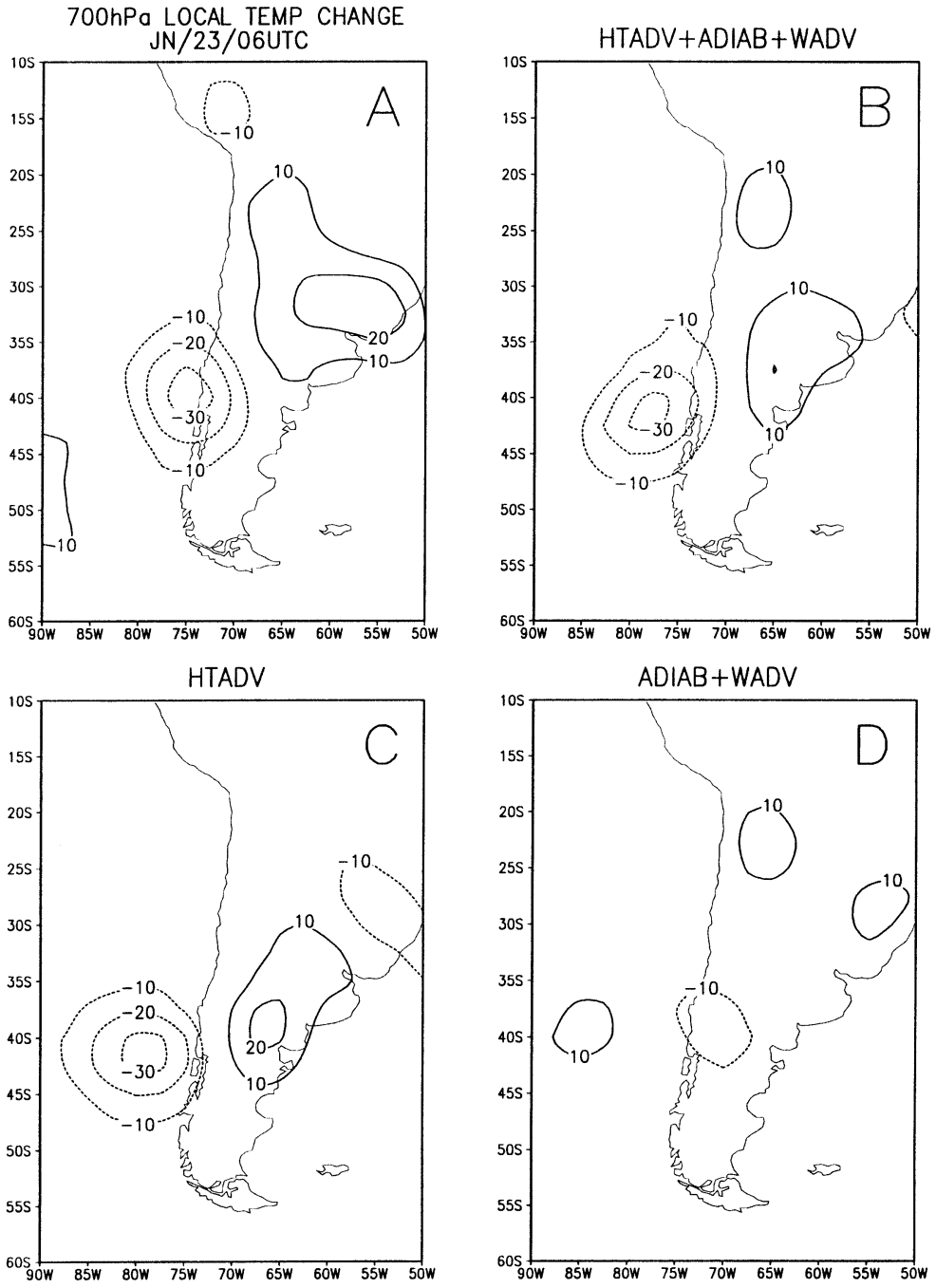

FIG. 13. Diagnosis of the thermodynamic equation at 700 hPa showing (a) local temperature change, (b) horizontal temperature advection (HTADV) plus adiabatic heating (ADIAB) plus vertical temperature advection (WADV), (c) HTADV, and (d) ADIAB+WADV. Units are 10^{-5} K s^{-1}.

zones. As in the starting phase [section 5a(4)], in the current section we will present evidence that those features influence the atmospheric flow at higher levels. In Figs. 16a, b the 500-hPa height evolution (Hovmoeller diagram) is related to the temperature advection C term (shaded) in the QG tendency equation [Eq. (3)]. Notice that the upper-level ridge (trough) intensified as it moved eastward in association with the warm (cold) advection below, indicated by the negative (positive) C terms. This suggests that the thermal advections mentioned previously would produce important effects at higher levels. To reinforce the idea, Fig. 16d shows that the upper-level trough was above the cold advection area (shaded), which

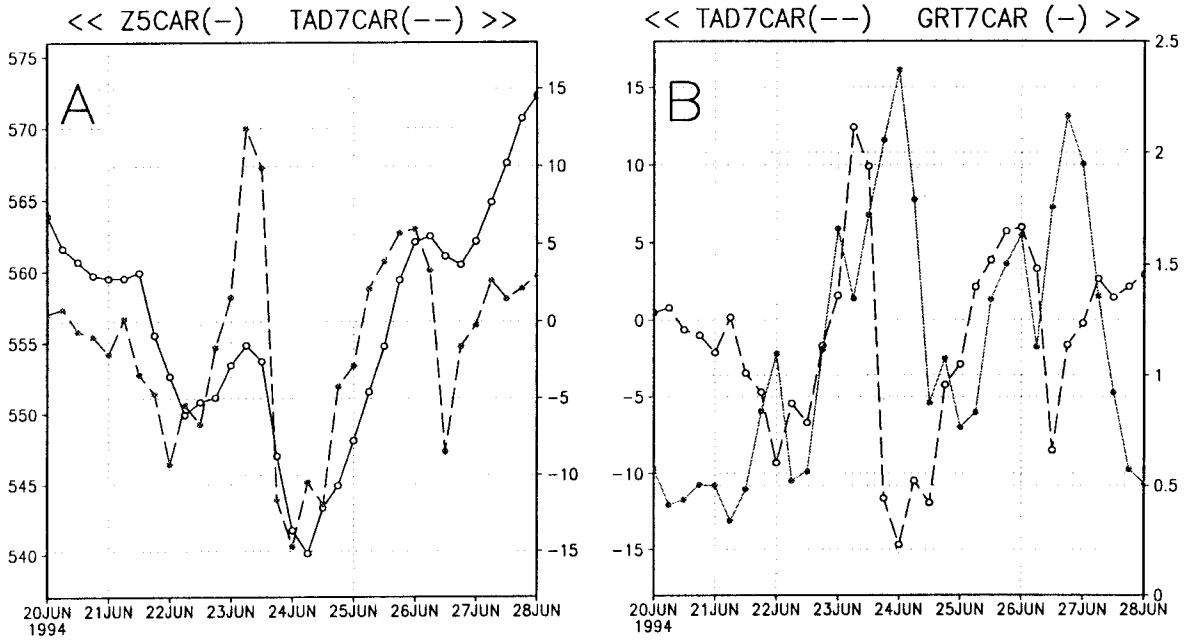

FIG. 14. (a) Time series of the CAR area (Fig. 1) averages of 500-hPa geopotential height (Z5CAR) (m) and 700-hPa horizontal thermal advection (TAD7CAR) (10^{-5} K s^{-1}). (b) Time series of TAD7CAR and the CAR area average of the square of the absolute value of the temperature gradient (GRT7CAR) (km^{-1}).

was in a location eastward of the cold tongue, as the 1000–500-hPa thickness field indicates.

2) LOW-LEVEL ANTICYCLOGENESIS AND CYCLOGENESIS

In this section we will be referring to the mechanisms for the formation of the surface high (low) SLP that is shown in dark (light) shading in Fig. 17a during the SB coldest day, upstream (downstream) of that region (Fig. 1). An index, Z85H (Z85L), was defined as the corresponding 850-hPa height average over the surface high (low). To indicate its local growth rate, we define Z85HCH (Z85LCH) as the average 12-h geopotential height change.

With respect to the formation of the low pressure, we have seen in section 5a(1) that, during the starting period near the Andes, it was associated with a CVA signal from an upper-level trough. In this section we will test the hypothesis that during the developing period, when the upper-level trough is deepening, the same mechanism may be working. We also define a new index, VORTAD3, over the surface low (SL) area (Fig. 1) as the corresponding 300-hPa vorticity advection average. In Fig. 17b, the time series of VORTAD3 and Z85LCH are shown. Notice that periods with CVA, indicated by negative values of VORTAD3, were associated with 850-hPa height drops represented by negative Z85LCH, suggesting that the CVA forcing would have been a main control over the near-surface low pressure in this zone. Notice also that during most of 25 June, the near-surface low pressure was locally being built up, as negative Z85LCH values were present. Another similar period was 21–22 June.

To analyze this relationship further, we used the QG omega equation [Eq. (4)] to determine VORTAD and TAD forcings in the vertical velocity. The corresponding indices in the SL area are W5VOADL and W5TADL, respectively, with their time series shown in Fig. 17c. In general, the former was larger than the latter. This was true mainly during the periods centered on about 25 June when the rate of near-surface low pressure local intensification was the largest. This fact would explain the close relationship between the VORTAD3 and Z85LCH shown in Fig. 17b.

With respect to the high SLP (SH), it may be formed when descending motions associated with low-tropospheric cold air advection tend to produce local anticyclonic vorticity time changes and height rises in near-surface levels. To test this hypothesis we defined two other indices over the SH area (Fig. 1). The TAD7H and Z85HCH are the SH averages of the 700-hPa temperature advection and the 850-hPa l2-h height change. In Fig. 18a, we present the time series corresponding to those indices. Not unexpectedly, they were out of phase; for example, negative (positive) TAD7H was associated with positive (negative) values of Z85HCH. If we take into account that the coldest day of the episode was 26 June, we may notice that during the two previous days the anticyclone was being built up in association with low-level cold advection as TAD7H indicated. To test the hypothesis further, we defined the index VV85H as the average 850-hPa p vertical velocity over the SH

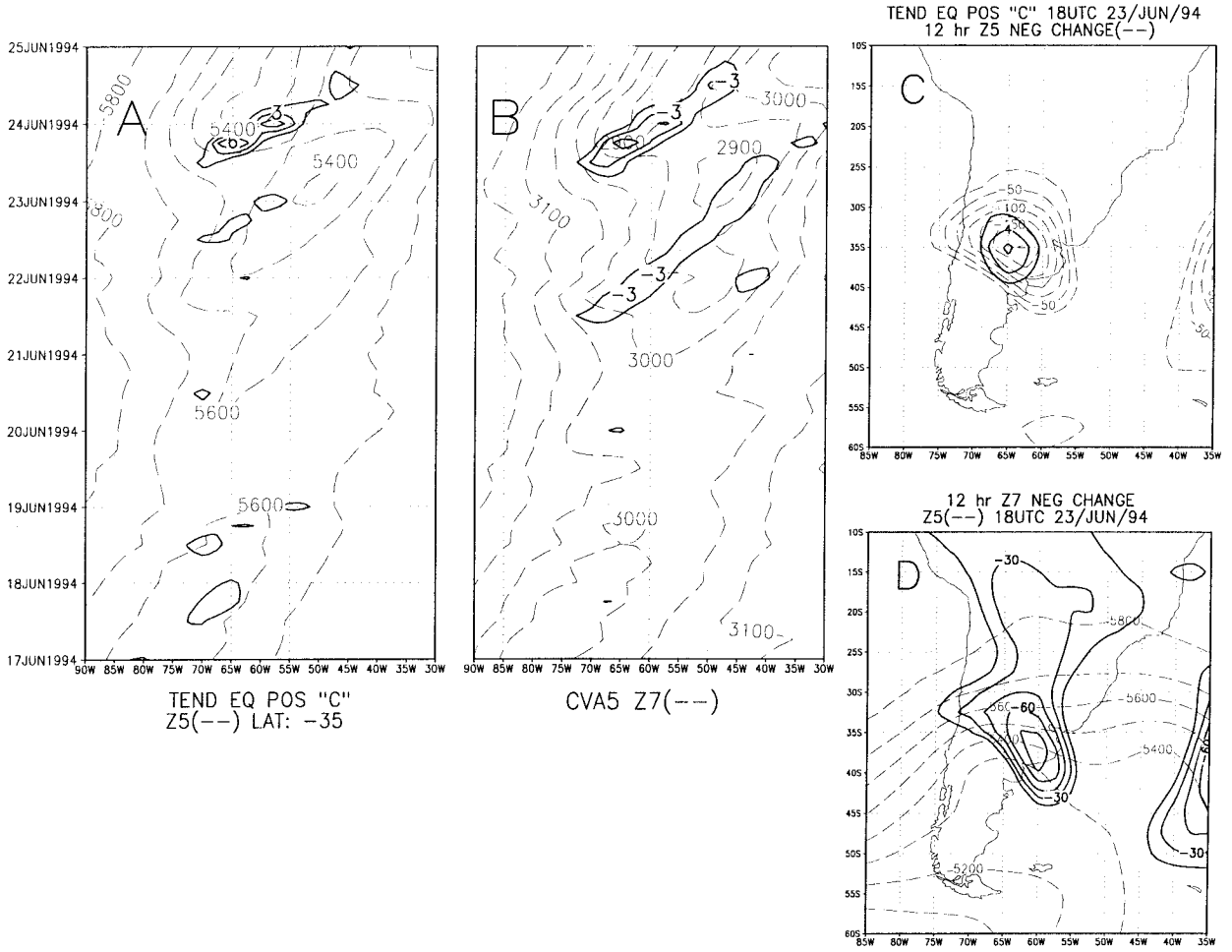

FIG. 15. (a) Evolution (Hovmoeller diagram) of 500-hPa height (dash, m, interval 100 m) at 35°S and of the QG geopotential height tendency equation C term [Eq. (3)] (solid, 10^{-13} s^{-3}, interval 1.5×10^{-13} s^{-3}). (b) Same as (a) except for 500-hPa CVA (solid, 10^{-9} s^{-2}, interval 1.5×10^{-9} s^{-2}), 700-hPa height (dash, m, interval 50 m). (c) 500-hPa 12-h negative height change (dash, m, interval 25 m), positive QG geopotential height tendency equation C term [Eq. (3)] (solid, 10^{-13} s^{-3}, interval 2×10^{-13} s^{-3}). (d) 500-hPa height (dash, m, interval 100 m), 700-hPa 12-h negative height change (solid, m, interval 15 m).

area. In Fig. 18d we present the time series corresponding to TAD7H and VV85H indices. Notice that the low-level cold advection period, indicated by a negative TAD7H swing during 24 June, was in general associated with positive values of VV85H, suggesting that descending motions were being mostly produced during this period. On a spatial domain, the local intensification of the near-surface anticyclone is shown in Fig. 18b. The vorticity equation terms HVOAD and DIVTERM [Eq. (2)] are shown in Figs. 18e and 18f, respectively, while their sum is presented in Fig. 18c. Notice that in general the equation is a reasonable approximation near the SH region as the local anticyclonesis is mostly explained with the considered terms. Notice also that positive values of the local 850-hPa vorticity change occurring near the SH area are due in large extent to the DIVTERM (Fig. 18e) confirming the proposed hypothesis.

Another noticeable feature is the low-tropospheric ridging near the eastern Andes' slopes, mainly in latitudes corresponding to Peru and Bolivia (Fig. 6h). Figure 19 shows the 850- and 925-hPa geopotential heights as well as the temperature and wind fields for a typical day with this feature. Notice that due to the cooling in the lee of the Andes, the isotherms tend to become oriented parallel to the mountains just east of the barrier. The low-level ridging over southern South America east of the Andes results in low-level easterly flow toward the mountains equatorward of the anticyclone center. As the air approaches the Andes, it is blocked and channeled equatorward down the pressure gradients, analogous to cold air damming signatures over North America (Bell and Bosart 1988; Keshishian et al. 1994).

3) PROPOSED NEAR-SURFACE COOLING MECHANISM OVER SOUTHEASTERN BRAZIL

A near-surface temperature index in the SB region (Fig. 1), TSB, was defined as the average 850-hPa

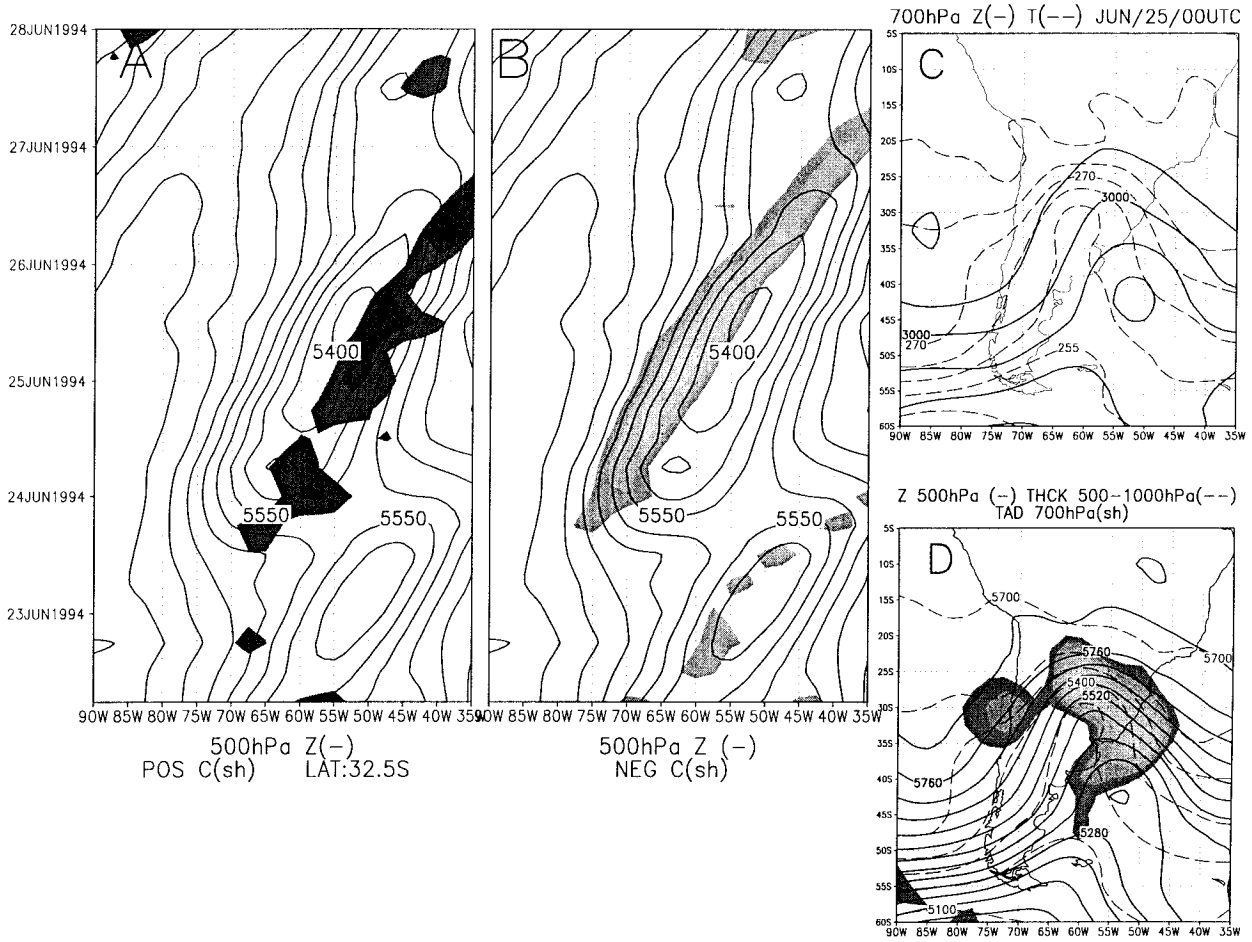

FIG. 16. (a) Evolution (Hovmoeller diagram) of 500-hPa height (solid, m, interval 50 m) at 32.5°S. Dark shading represents positive values of the QG geopotential height tendency equation C term [Eq. (3)]. (b) Same as (a) except that light shading represents negative values of the QG geopotential height tendency equation C term. (c) 700-hPa height (solid, m, interval 100 m), temperature (dash, K, interval 5 K). (d) 500-hPa height (solid, m, interval 60 m), 500–1000-hPa thickness (dashed, m, interval 100 m). Shading represents 700-hPa cold advection areas.

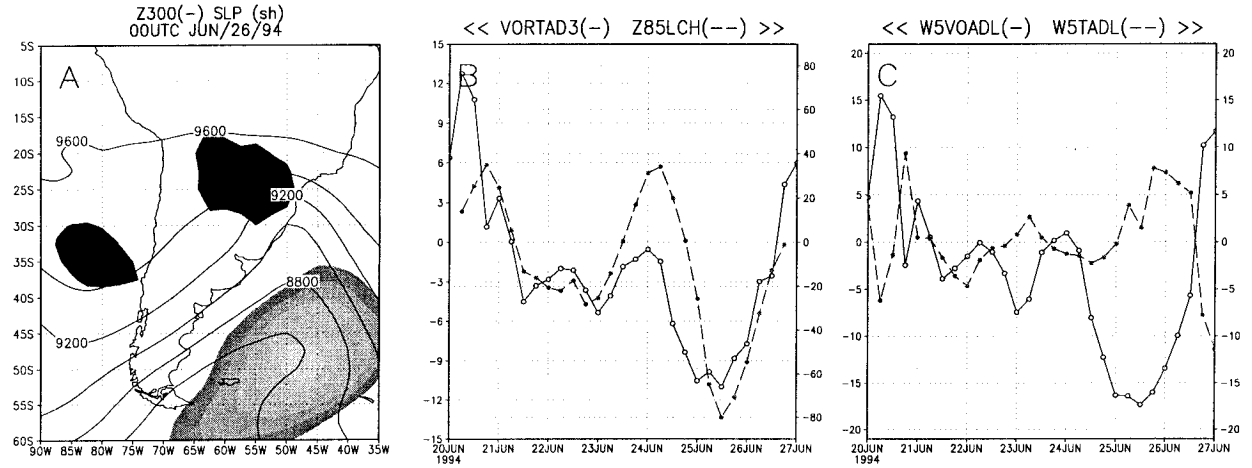

FIG. 17. (a) 300-hPa height (solid, m, interval 200 m). Dark (light) shading represents high (low) SLP. (b) Time series of the low SLP area averages of 300-hPa vorticity advection (VORTAD3) (10^{-10} s^{-2}) and the 850-hPa 12-h geopotential height changes (Z85LCH) (m). (c) Time series of the low SLP area averages of the differential vorticity advection term in the QG omega equation [see Eq. (4)] (W5VOADL) (10^{-13} Pa m^{-2} s^{-1}) and the thermal advection term in the same equation (W5TADL) (in 10^{-13} Pa m^{-2} s^{-1}).

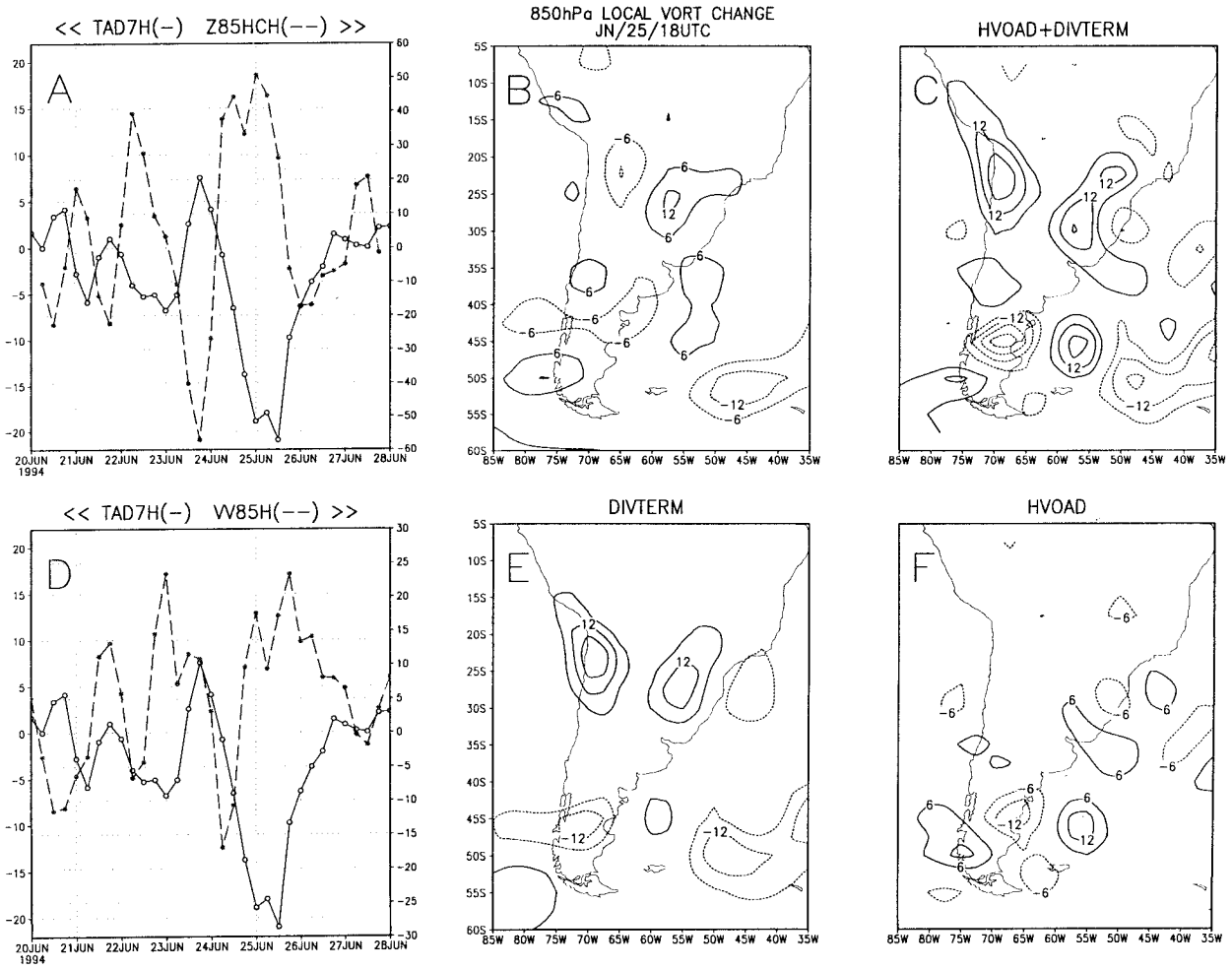

FIG. 18. Local anticyclogenesis at 850 hPa. (a) Time series of the SH averages of 700-hPa temperature advection (TAD7H) (10^{-5} K s^{-1}) and of the 850-hPa 12-h height change (Z85HCH) (m). Diagnosis of the vorticity equation at 850 hPa. (b) Local vorticity change. (c) HVOD + DIVTERM. (d) Time series of the TAD7H index (solid, 10^{-5} K s^{-1}) and of the SH average of the 850-hPa p vertical velocity (VV85H) ($100 \times$ Pa s^{-1}). (e) DIVTERM. (f) HVOAD (10^{-10} s^{-2}).

temperature. A significant 12°C TSB drop, which took place in the period 18/24–12/26, can be seen in Fig. 20a. In the same figure, notice that the Z5CAR index, which is an indicator of the 500-hPa height in the CAR area, had its minimum value on 24 June, about 48 h before the lowest temperature was observed in SB.

Figure 17a shows the 300-hPa geopotential height field, together with the high and low SLP (shaded) during the coldest day in SB. The orientation of these two features indicates that near-surface southwesterly winds would have been produced to transport cold air to SB from southern latitudes. Figure 20b shows the TSB and Z85H–Z85L time series, suggesting that the lowest SB temperatures were associated with a maximum in the near-surface height gradients. As indicated by the difference between Z85H and Z85L, southwest winds were produced to advect cool air from higher latitudes to SB.

c. Comparison of cases

In this section we present results regarding why some particular episodes are able to transport cold air more equatorward.

We selected strong (S) and moderate (M) events according to the intensity of the associated TSB index drop. Taking into account that, especially during the strong cases, the temperature fall usually is produced during an event-dependent time period; the only requirement in the classification is that the TSB drop occurs quasi-continuously with no restriction about the period of time in which such fall takes place. Values in the range 8°–12°C and 2°–4°C correspond to the S and M classes, respectively. As presented before (Fig. 14a), one characteristic of the TAD7CAR index is that it remained negative for some days before the coldest day of the event took place. To take into consideration the intensity of this cold advection as well as its duration,

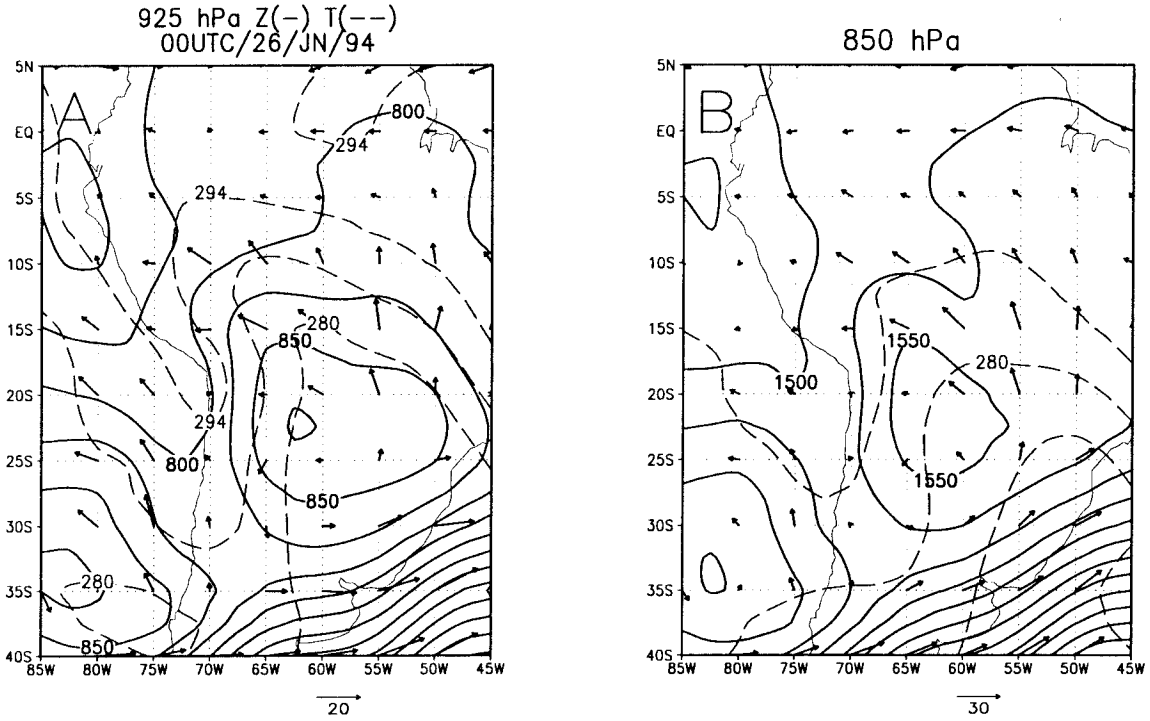

FIG. 19. (a) 925-hPa height (solid, m, interval 25 m), temperature (dash, K, interval 7 K) for 0000 UTC 26 June 94. (b) Same as (a) but for 850 hPa. Arrows represent the wind vector.

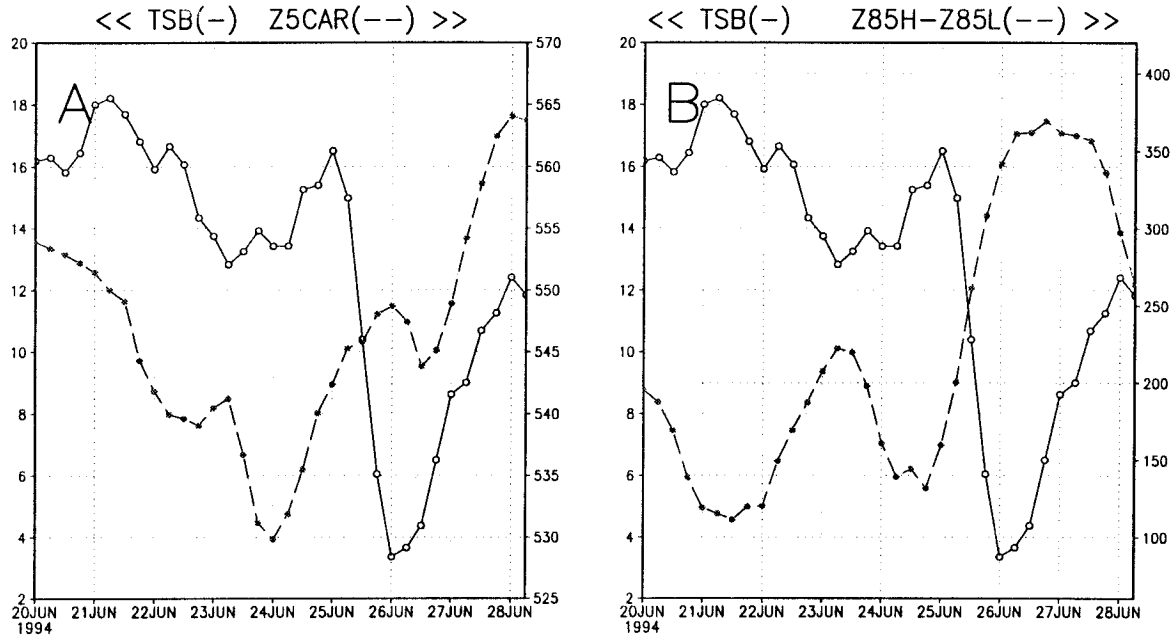

FIG. 20. Time series of (a) TSB (°C, solid), which is an 850-hPa temperature in an area, SB (Fig. 1), in southeastern Brazil, and of Z5CAR (dash, m), which is 500-hPa geopotential height for an area, CAR, near central Argentina (Fig. 1). (b) TSB (solid, °C) and of Z85H–Z85L, the 850-hPa height difference between SH and SL (Fig. 1) 850-hPa average height (dash, m).

TABLE 3. Intensity of cold episodes in southeastern Brazil (SB), as related to cooling (COOLCAR) in the central Argentina area (CAR). TSBDR indicates the total drop of the 850-hPa SB air temperature and S (M) corresponds to episodes of strong (moderate) intensity.

Date	COOLCAR (K)	TSBDR (K)	Class
8 June 1985	−19.27	11.0	S
9 May 1987	−19.11	9.0	S
26 May 1988	−10.92	7.0	S
13 July 1988	−12.13	9.0	S
26 July 1988	−8.87	10.0	S
27 May 1989	−6.45	8.0	S
7 July 1989	−14.45	9.0	S
19 June 1985	−3.59	4.5	M
10 June 1987	−4.22	4.0	M
18 May 1988	−4.10	4.0	M
9 May 1990	−2.61	2.5	M
13 May 1990	−5.73	3.0	M
4 July 1991	−5.40	4.0	M
3 July 1992	−2.75	3.0	M

a new index, COOLCAR, was defined as the time integral of TAD7CAR during the cold period previous to the coldest SB day.

Then, for each episode, the following characteristics were considered: the COOLCAR index, the TSB drop (TSBDR), and the class intensity, which all are shown in Table 3. The results indicate that the S episodes had a more negative COOLCAR index, significant at the 0.01 level, suggesting that the cooling east of the Andes during the starting phase would be a good early indicator of the intensity that low temperatures would reach later.

To find atmospheric features precursors of an S episode, we compared the 500-hPa height field evolution for the 26 June 1994 case (see Fig. 9) with that corresponding to another very weak (W) event during the period 17–19 June 1994, with almost no cooling observed in SB, although some may have been noticed at higher latitudes. It has already been shown in Fig. 9b that a trough intensified when reaching the Andes as it was moving eastward during the last week in June 1994. In contrast, during the weaker event a vorticity center of similar intensity did not intensify as it crossed the mountains (Fig. 21), possibly due to the weaker zonal winds as the S (W) event was of a westerly (northwesterly) type. Due to the more intense deepening, a more substantial CVA signal was produced in the S episode, with more intense low-level pressure drops. Consequently, stronger southerlies would have been present west of the Andes with colder advection.

5. Discussions

a. Physical mechanisms

Figure 22 is a schematic representation of the different processes during the starting (shaded) and developing periods in our case study. In our discussion, we will call day 0 the coldest day in southeastern Brazil. Similarly, day $-n$ ($+n$) will be the n day before (after). Square brackets refer to the different instances indicated by numbers in Fig. 22. Based on the results presented in the previous sections, the following scenario for the phenomena is suggested.

During about day −4, a short-wave upper-level trough was present west of the Andes around central and southern Chile in the Pacific Ocean, moving eastward toward the continent. In response to the approaching trough, and due to the association between ascending motion [2; 700 hPa] with substantial CVA aloft [1; 500 hPa], a significant SLP drop was produced initially at the western flank of the Andes and later on the other side [3; SURF]. During days −3 and −2, near-surface equatorward cold transport, due to the associated southerlies channeled by the Andes, was being produced [4; SURF].

At the same time, due to the same upward motion [2; 700 hPa] during days −4 and −3, a trough deepening near the 700-hPa level tended to occur near the Andes [3; 700 hPa]. As a consequence, due to advective [4; 700 hPa] and also adiabatic effects, a near 700-hPa cooling took place along the Andes [5; 700 hPa], which increased the zonal temperature gradients east of the cooling area [6; 700 hPa].

In turn, the low-tropospheric cold advection may also partially drive important changes in the upper-level flow pattern. Through contributing descending motions occurring behind the ascent region described in the previous paragraph, it may induce convergence and cyclonic time changes at those higher levels. We propose that this latter process together with the one described in the previous paragraph are the two parts of a positive feedback mechanism between the CVA in the upper flow and low-level troughing in association with cold advection due to the related southerlies.

The end result of this period was to have, at day −2, a deep trough in the lower troposphere from about 600 hPa to the surface east of the Andes at about 65°W that would let cold air be transported eastward [7; 700 hPa] to amplify the upper trough [8; 500 hPa] during days −1 and 0, due to the associated descending motions with upper-level convergence, cyclonic vorticity changes, and height drops during the developing phase. At the same time, near-surface anticyclogenesis [8; SURF] was associated with near 700-hPa cold advection [7; 700 hPa] through the descending motion with low-level divergence, anticyclonic vorticity changes, and height rises. Conversely, the near-surface cyclogenesis [9; SURF] was related to the upper CVA [8; 500 hPa] through the ascending motions and low-level pressure drops.

The system moved eastward, eventually reaching SB, producing significant temperature drops there. Our analysis suggests that the low SB [11; SURF] temperatures would be produced at least partially by advective process [10; SURF] related to the adequate location and intensity of the near-surface anticyclogenesis and cyclogenesis regions ([8; SURF] and [9; SURF]).

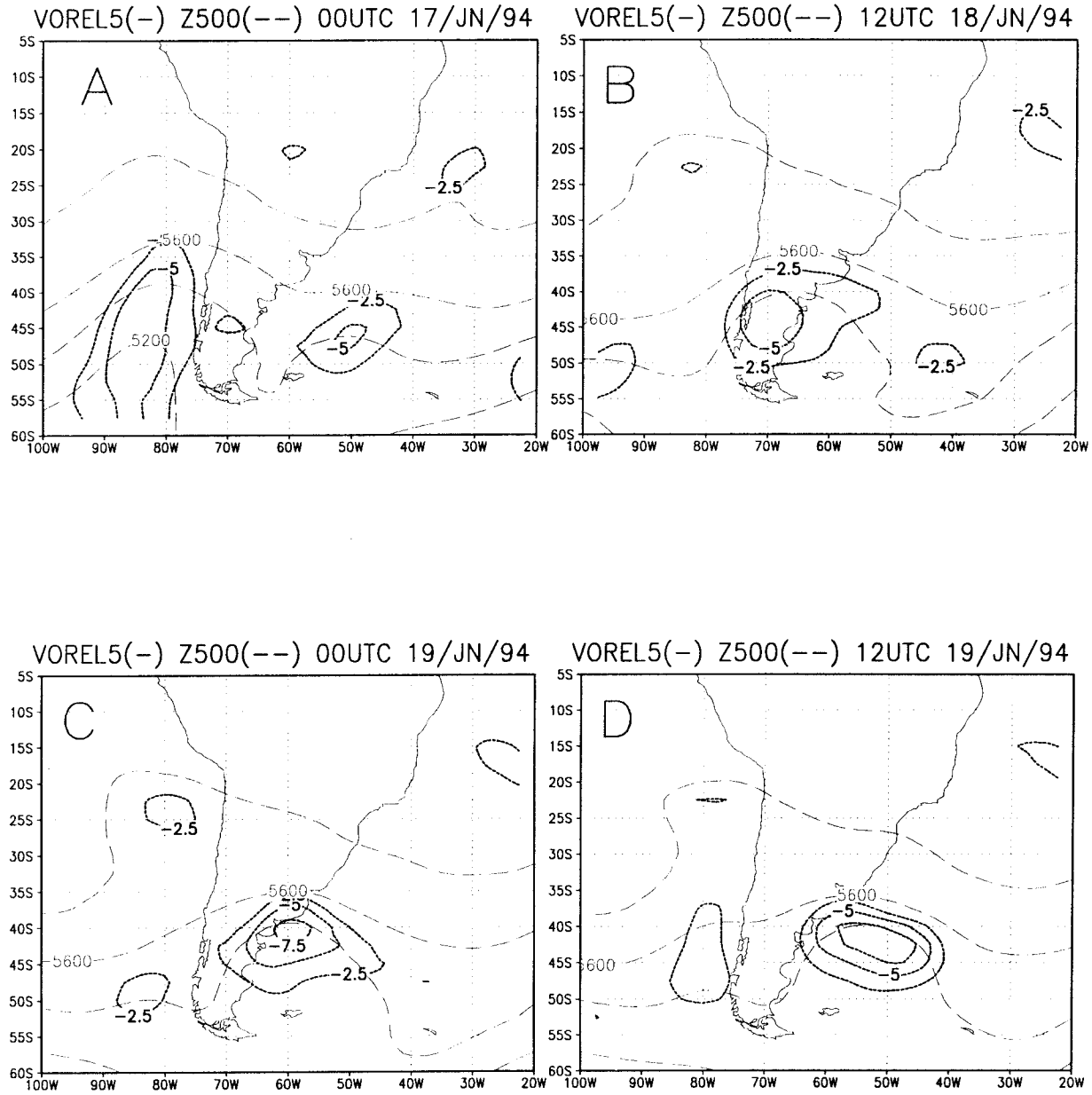

FIG. 21. Same as Fig. 10, but for other weak event.

With respect to the proposed positive feedback described earlier in this section, we would like to add some other details. Suppose a somewhat weak upper trough is just entering South America on central and/or southern Chile latitudes from the Pacific Ocean. As a result, some low-level height falls would take place first west and then east of the Andes due to the associated ascending motion. When located in the east of the Andes, its channeling effect would let a more effective equatorward cold-air transport by channeling the southerlies, which would show up between the mountains and the falling height region. The low-tropospheric cold advection would be partially responsible for a local deepening of the upper trough [C term in Eq. (3)]. According to the QG tendency equation, the upper-level vorticity advection [B term in Eq. (3)] is the other contributor to such deepening. The former is due to contributions from cold advection at lower levels, while the latter depends on vorticity advection at the same level. In the present event both terms were of similar importance (not shown). The same idea is true with respect to the vertical velocity. According to the QG omega equation [Eq. (4)], the vertical velocity depends on contributions from vertical variations of the vorticity advection (VORTAD term) and from the temperature advection field at the same level (TAD term). Even with the low-tropospheric

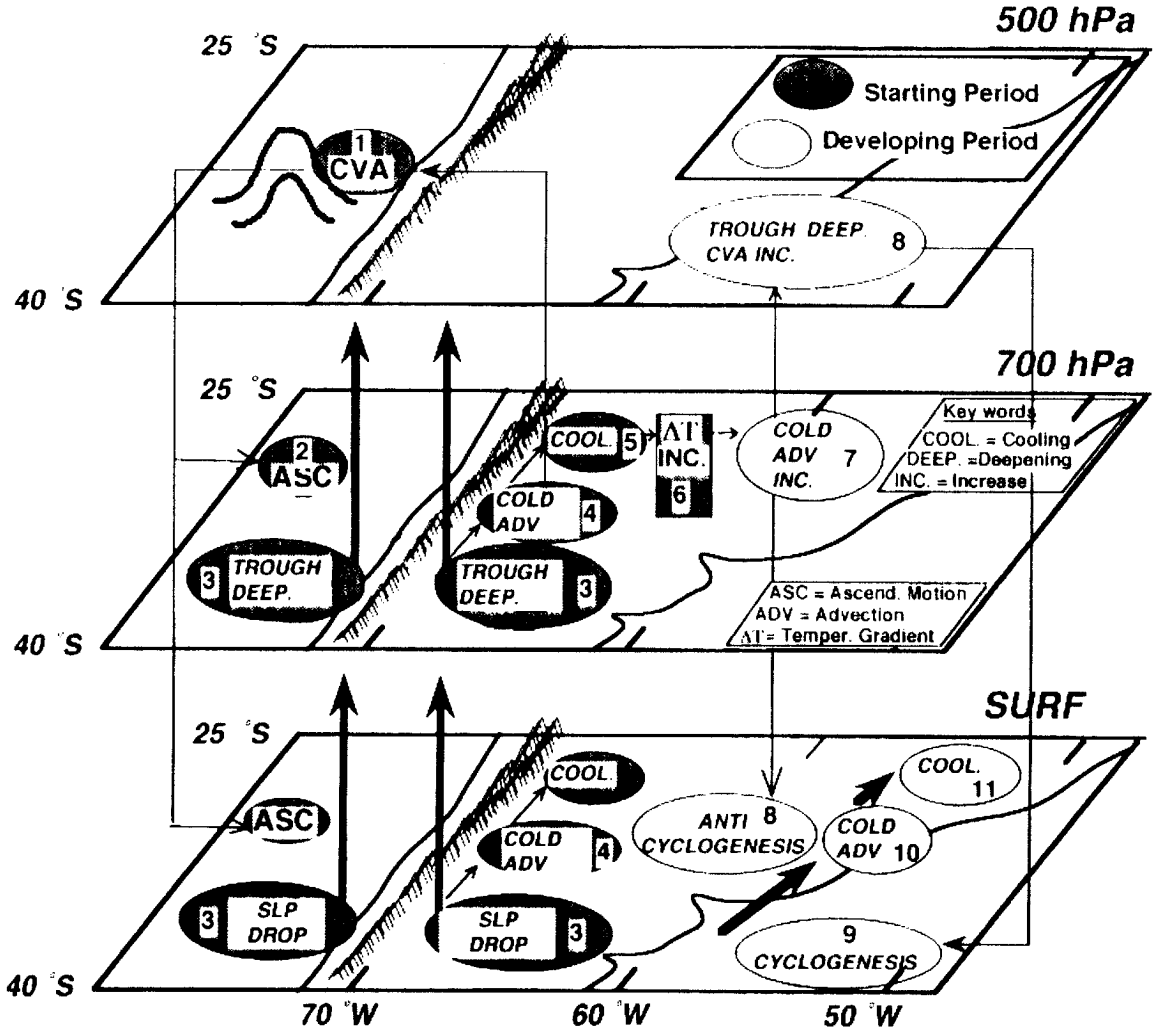

FIG. 22. Conceptual model. Schematic representation.

cold advection contributing to descending motions, the dominant upper CVA forcing [VORTAD term in Eq. (4)] indicates ascent.

The intensifying CVA signal ahead of the upper-level trough would intensify the ascending motions with larger low-tropospheric height falls, which would produce stronger equatorward cold-air transports. In return this would induce a more intense upper trough with more intense cold advections underneath and so on. In sum, a positive feedback mechanism.

In the present scenario, the Andes would play an important role by making possible a more effective equatorward transport of cold air by its channeling effect.

b. Comparison of the cases

Our results suggest that intensification of upper-level troughs that move eastward in mid- and high latitudes upon reaching the Andes is a characteristic of an event able to transport cold air farther equatorward. Although the reasons for such intensification deserve closer study, apparently it would be more possible for waves with stronger zonal velocities (Hartjenstein and Bleck 1991), such as the westerly type in the last week of June 1994, to be intensified as they cross the Andes. Such amplification would produce a more significant upper-level CVA signal with the corresponding larger upward vertical velocities and low-level pressure drops. Consequently, stronger cold advection would be transported equatorward by southerly winds along the eastern flank of the Andes. As shown in earlier sections, this cooling is essential in the development of several process that eventually lead to the production of low near-surface temperatures in SB.

In this respect, Figs. 15a, b, which were designed to present some evidence for the proposed positive feedback that would take place near the Andes during the starting phase in the S event 26 June 1994 case, also include the corresponding features for the W event that occurred in the period 17–19 June 1994 and was dis-

cussed in connection with Fig. 21. Notice that in this latter episode the positive feedback was not present, suggesting that this mechanism may be important in determining the future intensity of the event.

6. Conclusions

Cold surges affect southeastern Brazil during wintertime, sometimes leading to huge losses in coffee production and worldwide increases in prices. These waves may also penetrate into the Amazon region, producing cooling in southern and western Amazonia. The physical causes are related to the entrance of a cold-core anticyclone from the eastern Pacific into South America, then passing over the Andes and moving northward along the eastern flank of the mountains. Whenever the anticyclone reaches its northernmost position nearby southeastern Brazil, cold weather affects this region, and the cold air is expected to arrive in southern Amazonia 24 h later. Time series of surface weather elements in June 1994 show the advance of the cold air toward the equator that did not affect central and eastern Amazonia, while western and southern Amazonia observed marked decreases in air temperature. At upper levels, the movement of a ridge–trough system from the eastern Pacific preceded the entrance of cold air into southeastern Brazil. When the trough reached southern Brazil, it intensified during the coldest day in this region, while the ridge was located along Chile.

Based on the analysis of climatic time series in southeastern Brazil and Amazonia and on the dynamic aspects of the cold surges described here, the following conclusions can be drawn.

1) Our results suggest that the strong southeastern Brazil (SB) cold outbreak would be associated with an intense positive feedback mechanism between upper and lower atmospheric flows near the Andes in central and southern Chile prior to the coldest day. Consequently, intense troughing is produced in the lee of the Andes at those latitudes with the associated low-level cold advection due to southerlies along the eastern flank of the mountains. It seems that the same intensity of the feedback would also be related to the lower latitude the cold air would reach later. The analysis of more events will let us to obtain more firmer conclusions.
2) A region called CAR (Fig. 1) would then be very important in the monitoring and predicting cold events over SB. The average 500-hPa geopotential height (Z5CAR) and 700-hPa temperature advection (TAD7CAR) defined in the area would be precursors of the episodes. About 48 h after those indices reached a minimum value, a cold event would occur over SB. Our study suggests that the time integral of the latter index over the period of time in which it remained negative previous to the coldest day (COOLCAR index) would be related with the future cooling intensity over SB. This means that only those events with enough negative COOLCAR index value are able to penetrate to lower latitudes. At the other extreme, those episodes with weak negative COOLCAR would produce cooling effects only at higher latitudes. The channeling effect of the Andes could be crucial in the production of cold advection east of the mountains, which is also decisive in the development of the proposed feedback mechanism.
3) Our results suggest the possibility that the cold-air damming effect explains the ridging along the eastern flank of the Andes as in similar cases in the world. This feature is important in advecting cold air to western Amazonia. To further study this phenomena, a deeper analysis with higher time and space resolution is needed.
4) Our results have also suggested a mechanism for the evolution of the cold episodes. It includes the early presence of an upper-level trough moving into the continent from the Pacific in mid- and/or high latitudes. During the starting period several processes are conducive to the intensification of the zonal temperature gradients in the lee of the Andes, which permit production of eastward cold air transports during subsequent days. This latter feature would be partially responsible for the observed upper-level wave amplification.

Acknowledgments. Thanks are due to Sergio and Nury Calbete from CPTEC/INPE, to Iclea and Ernesto Grammelbacher from INMET, and to Eng. Roberto Thomaziello from the Secretaria de Agricultura e Abastecimiento of the state of São Paulo, Brazil, for supplying the surface and upper-air charts, the synoptic information, and data on coffee production. We also thank the Sistema Meteorologico de Paraná (SIMEPAR) from the state of Paraná, Brazil, and the people from the ABRACOS Experiment for providing daily weather information for sites in southeastern. Brazil and Amazonia, respectively. We also acknowledge the National Climatic Data Center from Asheville, North Carolina, for providing the daily climatological data as well as the surface and upper-level charts for the case study, and NCAR–UCAR for providing the NCAR–NCEP reanalysis data. We wish to thank the help from Prof. T. Krishnamurti and L. Bosart from FSU and SUNY, respectively, for reading earlier versions of this manuscript.

This research was done with the support of the Conselho Nacional de Desenvolvimiento Cientifico e Tecnologico (CNPq) of the Ministerio de Ciencia e Tecnologia of Brazil, through its Program RHAE fellowships for Jose A. Marengo and Angel G. Cornejo at the CPTEC/INPE, in Cachoeira Paulista.

REFERENCES

Algarbe, V. R., and I. Cavalcanti, 1994: Caracteristicas da Circulacão atmosferica associadas a ocorrência de geadas no sul do Brasil.

VII Congresso Brasileiro de Meteorologia, 626 pp. [Available from Sociedad Brasileira do Meteorologia, Universidade Federal do Rio de Janeiro, Predio do CCMN-Bloco G. Cidade Universitaria, Rio de Janeiro, Brazil.]

Bell, G. D, and L. Bosart, 1988: Appalachian cold-air damming. *Mon. Wea. Rev.,* **116,** 137–161.

Brinkman, W., and M. N. Goes-Ribeiro, 1971: Air temperature in central Amazonia I. *Acta Amazônica,* **1** (1), 51–56.

——, and ——, 1972: Air temperature in central Amazonia III. *Acta Amazônica,* **2** (3), 28–39.

——, J. Weinman, and M. N. Goes-Ribeiro, 1971: Air temperature in central Amazonia II. *Acta Amazônica,* **1** (3), 27–32.

Colucci, S. J., and J. C. Davenport, 1987: Rapid surface anticyclogenesis: Synoptic climatology and attendant large scale circulation changes. *Mon. Wea. Rev.,* **115,** 822–836.

Colle, B. A., and C. Mass, 1995: The structure and evolution of cold surges east of the Rocky Mountains. *Mon. Wea. Rev.,* **123,** 2577–2610.

Dapozzo, J., and M. A. F. Silva Dias, 1994: Um estudo de caso da penetracao do ar polar em latitudes baixas: Julho de 1988. VII Congresso Brasileiro de Meteorologia, 626 pp. [Available from Sociedade Brasileira do Meteorologia, Universidade Federal do Rio de Janeiro, Predio do CCMN-Bloco G. Cidade Universitaria, Rio de Janeiro, Brazil.]

Fortune, M., and V. E. Kousky, 1983: Two severe freezes in Brazil: Precursors and synoptic evolution. *Mon. Wea. Rev.,* **111,** 181–196.

Gash, J. H. C., C. A. Nobre, J. Roberts, and R. Victoria, 1996: An overview of ABRACOS. *Amazonian Deforestation and Climate,* J. H. C. Gash, C. Nobre, J. Roberts, and R. Victoria, Eds., John Wiley and Sons, 1–14.

Girardi, C., 1983: El Pozo de los Andes (in Spanish). Preprints, *First Int. Congress on Southern Hemisphere Meteorology,* São Jose dos Campos, São Paulo, Brazil, Amer. Meteor. Soc., 226–229.

Haddock, D., R. Motta, R. McInturff, M. Halpert, and R. Smelser, 1981: Freeze hits Brazilian coffee area on July 20 and 21, 1981. *Weekly Wea. Crop Bull.,* **68** (30), 25–27.

Hamilton, M., and J. Tarifa, 1978: Synoptic aspects of a polar outbreak leading to frost in tropical Brazil, July 1972. *Mon. Wea. Rev.,* **106,** 1545–1556.

Hartjenstein, G., and G. Bleck, 1991: Factors affecting cold-air outbreaks east of the Rocky Mountains. *Mon. Wea. Rev.,* **119,** 2280–2292.

Holton, J. R., 1992: *An Introduction to Dynamic Meteorology.* Academic Press, 511 pp.

Kalnay, E., and Coauthors, 1996: The NCEP/NCAR 40-year reanalysis project. *Bull. Amer. Meteor. Soc.,* **77,** 437–471.

Keshishian, L., L. Bosart, and W. Bracken, 1994: Inverted trough and cyclogenesis over interior North America. A limited regional climatology and case studies. *Mon. Wea. Rev.,* **122,** 565–607.

Konrad, C. E., and S. J. Colucci, 1989: An examination of extreme cold air outbreaks over eastern North America. *Mon. Wea. Rev.,* **117,** 2687–2700.

Lichtenstein, E., 1989: Some influences of the Andes cordillera on the synoptic scale circulation. Preprints, *Third Int. Congress on Southern Hemisphere Meteorology and Oceanography,* Buenos Aires, Argentina, Amer. Meteor. Soc., 156–159.

Marengo, J., 1984: Estudio sinoptico-climatico de los Friajes en la Amazonia peruana (in Spanish). *Revista Forestal del Peru,* **12,** 55–80.

——, C. Nobre, and A. Culf, 1997: Climatic impacts of ''friagens'' in forested and deforested regions in Amazon Basin. *J. Appl. Meteor.,* **36,** 1553–1566.

Marshall, C. F., 1983: *The World Coffee Trade.* Woodhead-Faulkner, 254 pp.

Morize, H., 1922: Contribução ão Estudo do Clima do Brasil (in Portuguese). Ministerio da Agricultura, Industria e Commercio, Observatorio Nacional de Rio de Janeiro, 79 pp. [Available from Instituto Nacional de Pesquisas Espaciais, Sao Jose dos Campos, Caixa Postal 515, São Paulo, Brazil.]

Myers, V., 1964: A cold front invasion in southern Venezuela. *Mon. Wea. Rev.,* **92,** 513–521.

Parmenter, F., 1976: A Southern Hemisphere cold front passage at the equator. *Bull. Amer. Meteor. Soc.,* **57,** 1435–1440.

Rogers, J., and R. Rohli, 1991: Florida citrus freezes and polar anticyclones in the Great Plains. *J. Climate,* **4,** 1103–1113.

Satyamurty, P., P. Etchichury, C. Studzinsky, N. Calbete, R. Lopes, I. A. Glammelsbacher, and E. A. Glammelsbacher, 1990: A primera friagem do 1990: Uma descripção sinótica (in Portuguese). *Climanalise,* **5** (5), 43–51.

Schubert, S., J. Pfaendtner, and R. Rood, 1993: An assimilated dataset for earth science applications. *Bull. Amer. Meteor. Soc.,* **74,** 2331–2342.

Schultz, D., W. Bracken, L. Bosart, G. Hakim, M. Bedrick, M. Dickinson, and K. Tyle, 1997: The 1993 superstorm cold surge: Frontal structure, gap flow, and extratropical impact. *Mon. Wea. Rev.,* **125,** 5–39.

Seluchi, M., and J. Nery, 1992: Condiciones meteorologicas asociadas a la ocurrencia de heladas en la region de Maringa (in Spanish). *Rev. Brasileira Meteor.,* **7,** 523–534.

Serra, A., and L. Ratisbona, 1942: As massas de ar da America do Sul (in Portuguese). Ministerio da Agricultura, Serviço de Meteorologia, Rio de Janiero, 66 pp. [Available from Instituto Nacional de Pesquisas Espaciais, Sao Jose dos Campos, Caixa Postal 515, São Paulo, Brazil.]

Tarifa, J., H. Pinto, R. Affonsi, and M. Pedro, 1977: A gênese dos episodios meteorológicos de julho de 1975 e a variação espacial de danos causados pelas geadas na cafeicultura no Estado de São Paulo (in Portuguese). *Ciênc. Cult.,* **29,** 1362–1374.